Adsorption and Decomposition of Lignin Model Molecules: the Veratrol Family. A Surface Science Approach.

Mohammed Asiri

uOttawa

Thesis Submitted to the Faculty of Graduate and Postdoctoral Studies as Part of the Requirement for the M.Sc. Degree in Physics

Department of Physics, Faculty of Science,
University of Ottawa

Supervisor: Javier B. Giorgi

117 D'Iorio Hall, 10 Marie Curie, Ottawa ON Canada, K1N 6N5

Abstract

The growth of the World's population always comes with a higher demand of energy. Covering this demand requires finding new energy sources and especially ones that manage the risks of further global warming. Biomass energy is considered as one of the clean energy resources, and widely available. Lignin is a lignocellulosic biomass polymer that constitutes the second most abundant polymer in biomass. The interest of lignin in science laboratories is due to its availability and sustainability that could produce a new supply of fuels and valuable chemicals.

Among the different methods of lignin conversion into fine chemicals, heterogeneous catalysis seems to be a perfect method because it reduces the activation energies for reaction and it separates the product from the catalyst. In this work, the conversion of lignin by a heterogeneous catalyst was explored under ultrahigh vacuum conditions using three surface science techniques: Infrared Reflection Absorption Spectroscopy, X-ray Photoelectron Spectroscopy, and Temperature Programmed Desorption. Because of the difficulties of using lignin under UHV conditions due to its physical properties, lignin model molecules with the same chemical structure are the only way to gain better understanding of lignin reactivity. In the present work, Veratrol, 1,3-dimethoxybenzene, and 1,4-dimethoxybenzene were used on Pt(111) surface as lignin models.

The reactivity of veratrol on Pt(111) showed the formation of 1,2-benzoquinone by the dehydrogenation of the two methyl groups, which gave three desorption products: catechol (observed here for the first time), hydrogen, and carbon monoxide. The isomers 1,3 and 1,4 desorbed hydrogen and carbon monoxide of their monolayer desorption predictably. 1,3-dimethoxybenzene showed the formation of benzene at certain temperatures. 1,4-dimethoxybenzene adsorbed on Pt(111) via the carbon species of its aromatic ring.

The three isomers show slightly different adsorption geometries which lead to rather different decomposition pathways. This study of such complex behavior is a great example of the sensitivity of selectivity in heterogeneous catalysis, even for very similar isomers.

The detailed thesis is a continuous work of the route forwarding lignin valorization by increasing the complexity of the models of lignin.

Acknowledgment

First of all, thanks to Allah for everything given to me.

To my great father Zayed Asiri, I always try to do all my best to be proud of me as I am always so proud that I am a son of the greatest father.

To my beloved mother Shariefah Al-Saeed, your guidance and praying are the candle that lights all my routes in the life.

My Sincere thanks and deep gratitude to Dr. Javier Giorgi for giving me the best opportunity of my academic life. Your unlimited guidance, support, and encouragement make the work in laboratory really interesting. The person who stands with me at the moment when all my dreams faded away and he made them alive again and achievable. The period of my training was not plentiful enough but I have learnt many skills in both academic and practical life. No word in the dictionaries of all languages could describe my thankfulness to you Javier. Javier, you are the greatest man in my whole life beyond my father.

I would dedicate this work to my brothers Ali and Essa, to my three amazing sisters. To my Fiancée Nourah.

Special thanks to my friends: I would thank my friend Motieb Al-Otaibi who shared me this journey. A special thanks to Abakar Maloum who “opens his heart before ears” when I need to talk. Thanks to all my friends in Ohio, Ireland, and Saudi Arabia.

I have to thank my lab-mates for collaboration work: Aghiles Ould Hamou and Virgina Kusuma.

Great thanks to Elvira Evangelista who did all the best to push my admission application in tight period. Other huge thanks to Bela Joos “the Godfather” of all graduate students of Physics department.

Thanks to the science store people, workshop, and special thanks to Ian Mayer who helped a lot with FTIR.

I would also thank Saudi Cultural Bureau in Ottawa and my sponsor for financial support.

Table of Contents:

List of Figures

Chapter 1

Chapter 2

Chapter 3

Chapter 4

List of Tables

Chapter 1

Chapter 3

Chapter 4

List of Symbols and Abbreviations

Symbol/Abbreviation	Definition
UHV	Ultrahigh vacuum
IRAS	Infrared reflection absorption spectroscopy
XPS	X-ray photoelectron spectroscopy
TPD	Temperature-programmed desorption
LEED	Low-energy electron diffraction
HREELS	High-resolution electron energy-loss spectroscopy
RGA	Residual gas analyzer
QMS	Quadrupole mass spectrometer
MCT	Mercury Cadmium Telluride
MSSR	Metal surface selection rule
FTIR	Fourier-transform Infrared
SNR	Signal-to-noise ratio
$E_{binding}$	Binding energy
$E_{kinetic}$	Kinetic energy
E_{des}	Desorption energy
E_p'	Reflected Electric field with a perpendicular polarization
E_s'	Reflected Electric field with a parallel polarization
E_p	Electric field with a perpendicular polarization
E_s	Electric field with a parallel polarization

Θ	Surface coverage
Φ_s	Instrument work function
k_{des}	Rate constant of desorption
r_{des}	Rate of desorption
β	Rate of Heating
T	Temperature
T_o	Initial temperature
T_{max}	Maximum temperature
t	Time
P	Pressure
m	Mass
R	Gas constant
k_b	Boltzmann constant
h	Plank's constant
Z_w	Impingement rate
w	Wavenumber
λ	Mean free path
Z	Collison frequency
$\bar{\upsilon}$	Mean velocity
δ	Optical path difference
I	Beam intensity
IR	Infrared

P-	Perpendicular
s-	Parallel
σ	Cross section
N	Number of scans
Pt	Platinum
L	Langmuir

Chapter 1: Introduction

General Introduction and Research Approach:

1.1 Energy consumption

The demand of energy increases every year with the growing of the world population and nations becoming industrialized countries. Current sources of energy are primarily based on non-renewable, which are oil, natural gas, and coal. There are also renewable energy sources including biomass, geothermal, wind, hydropower and solar energy. It is worth mentioning that the main resources for world energy supply are the fossil fuels that constitute up to 85% of the world consumption, as shown in (Figure1.1).[1]

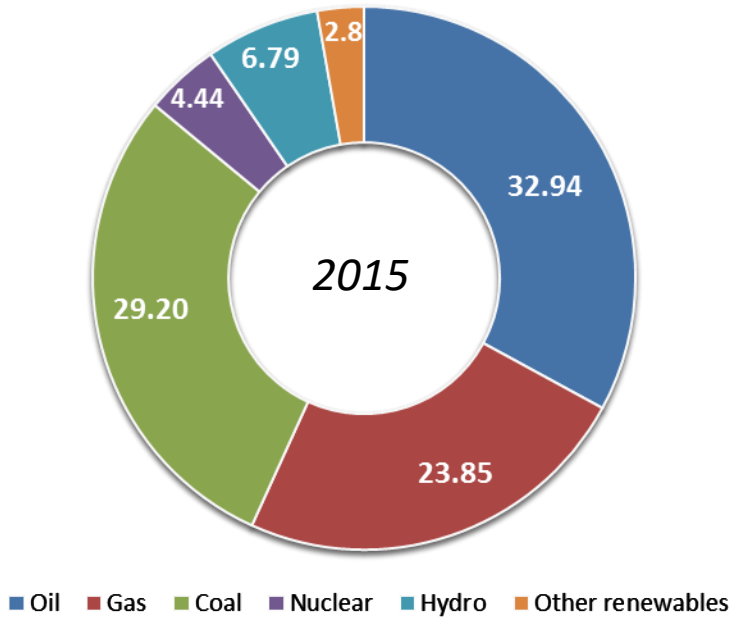

Figure 1.1*: The World energy consumption in 2015. Replotted from data published by World Energy Council.*[1]

Unfortunately, the nonrenewable energy resources are limited which means they have a depletion time. According to the current world's consumption of fossil fuels, their reserve depletion times for oil, natural gas and coal are approximately 34, 42 and 70 years, respectively.

This means the coal reserves are the only fossil fuel remaining after 2060, and will be available up to 2088 (Figure1.2).[2] Moreover, fossil fuels emit toxic gases during the burning process; they produce large quantities of carbon dioxide when they are burned. The pollution resulting from fossil fuels emissions increases global warming. Therefore, it is a necessity to find sources of energy that are sustainable and "eco friendly". Biomass seems to be the best candidate since it is a renewable and sustainable source of energy that can be used to create electricity or other forms of power. Plus, the biomass energy will reduce the greenhouse gas emission because burning biomass to create energy releases no new carbon back into the atmosphere.[3] Instead, it releases what would be released naturally as the organic matter decomposed.

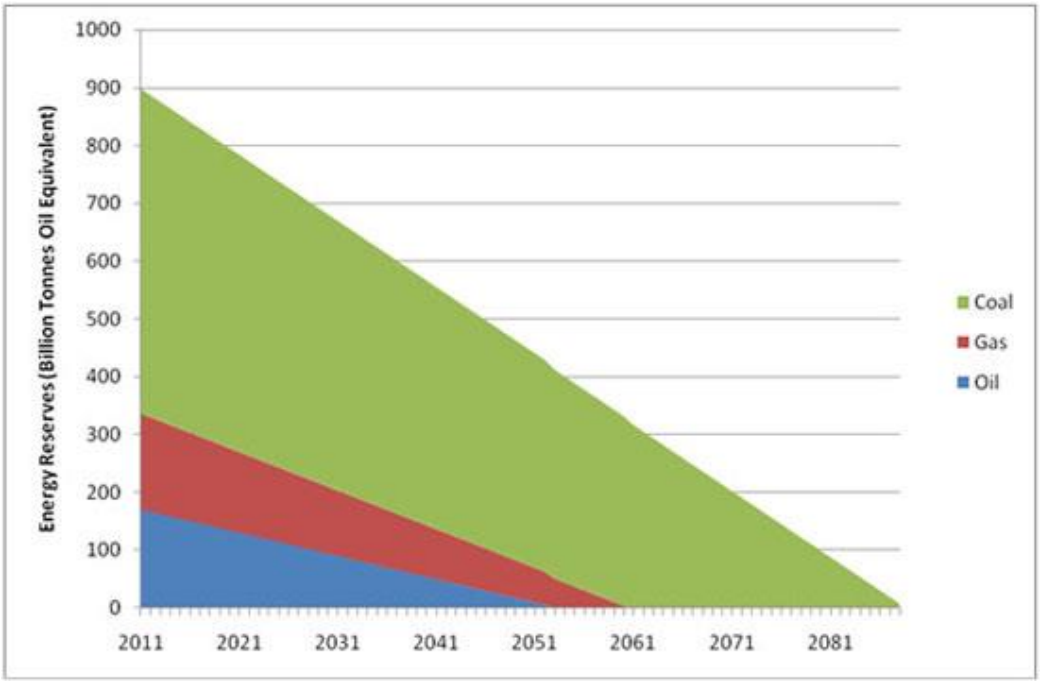

Figure 1.2: *Years of global coal, oil and natural gas left. Data from CIA World feedstock.*[2]

1.2 Biomass Energy

Biomass energy is defined as the energy that comes from organic materials that stock from plants including trees, seaweeds, animal wastes and crops. The resources of biomass energy are considered as the most abundant and widespread energy source in the World. The dry biomass is known as lignocellulose which consists of three major polymers: Cellulose, Lignin, and Hemicellulose.[4]

1.2.1 Lignocellulosic Biomass

Cellulose ranks as the most abundant polymer in lignocellulose.[5] Exploitation of cellulose is mainly to produce paper products. Cellulose can be also modified in many different ways to create new compounds that are useful in a variety of applications. In the biomedical field, it can be used as blood purification membranes and texturizer. Also, smaller quantities of cellulose are converted into synthetic fiber called rayon which is used in clothing.[6] While the second most abundant polymer in lignocellulose is hemicellulose,[5] the current uses of hemicellulose are limited to create some plasticizers. The mechanical strength of pure hemicellulose films can be improved by making composites with bio-based components.[7] At present, there is an increasing interest to develop new applications of hemicelluloses as raw materials for the chemical industry and also in the fields of food and pharmaceutical industries.[8]

Lignin which represents up to 30 percent of the lignocellulose biomass is a source of highly valuable compounds, which are currently produced from oil fractions like Benzene, Toluene and Xylene.[9] Next section (1.3) will present the lignin extensively.

1.3 Lignin

1.3.1. Definition and Historical Background

Lignin is an organic complex polymer that forms essential structural material in plants tissues and some algae, which gives the strength to the plant tissue stiffness to the cell wall. Also, it retains water and nutrients in the fibers.[10] Lignin is one of two major polymers in wood behind Cellulose and equally with Hemicellulose. Indeed, the lignin natural abundancy represents up to 24 – 33% and 19 – 28%, respectively, to dry wood weights of normal softwoods and temperate-zone hardwoods.[11] Biodegradation of lignin is slower and less complete than degradation of other organic polymers.[12]

The first mention of lignin was in 1813 by the Swiss botanist A.P. de Candolle who named lignin that is derived from the Latin word "lignum" meaning wood. His description of lignin was a fibrous and tasteless material that is insoluble in water and alcohol but soluble in weak alkaline solutions.[13]

1.3.2. Lignin Composition and Structure

The composition and amount of lignin varies from species to species, tree to tree, and even in woods from different parts of the same tree. An example of the elemental composition of lignin from an Aspen wood is 63.4% C, 5.9% H, 30% O (by difference), and 0.7% ash, corresponding approximately to the formula ($C_{31}H_{34}O_{11}$).[14] In general, the structure of lignin contains three different phenyl propane monomer units known also as *monolignols*, para-coumaryl alcohol, sinapyl alcohol, coniferyl alcohol (Figure1.3).[4] The polymer linkages consist of carbon-carbon bonds (*5-5*, *β-5*, *β-1*, *β-β*) and ether bonds (*β-O-4*, *α-O-4*, *4-O-5*, *α-O-γ*). The β-O-4 aryl ether bonds are the most frequent coupling linkage that formed up 60% of the whole lignin as shown in

(Table 1.1).[4] The typical structure of lignin showing the most common linkages is depicted in Figure 1.4.[15]

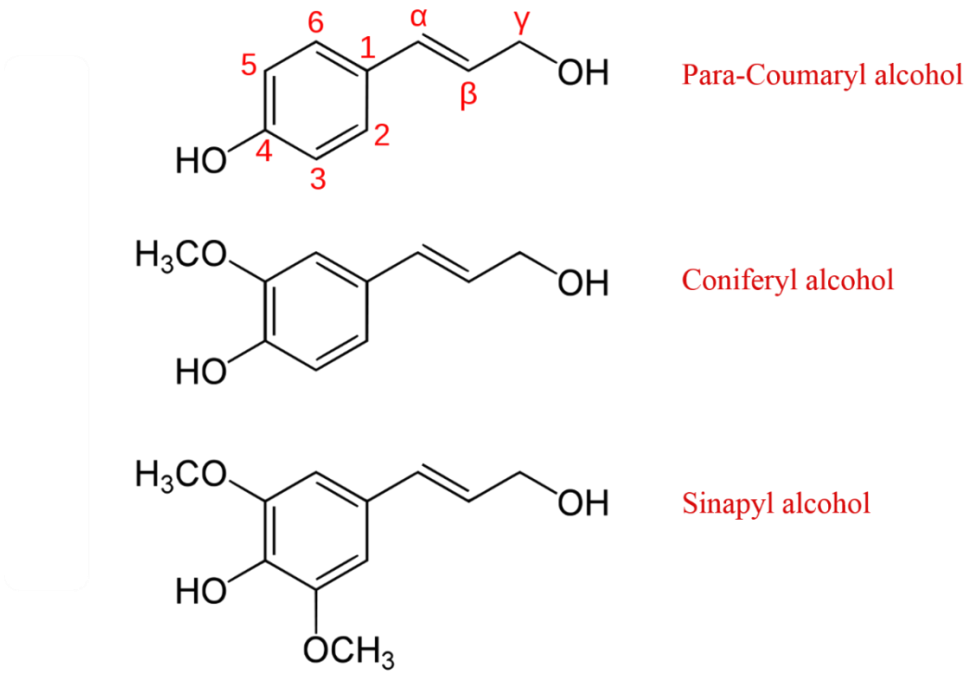

Figure 1.3: *Chemical structure of the three main monolignols that forms lignin.*

Table 1.1: *Proportions of major linkages of lignin.[4] Copyrights ©2010 John Wiley & Sons, Inc. Reprinted by permission of John Wiley & Sons, Inc.*

Linkage type	**Softwood [%] (spruce)**	**Hardwood [%] (birch)**
β-*O*-4-Aryl ether	46	60
α-*O*-4-Aryl ether	6–8	6–8
4-*O*-5-Diaryl ether	3.5–4	6.5
β-5-Phenylcoumaran	9–12	6
5-5-Biphenyl	9.5–11	4.5
β-1-(1,2-Diarylpropane)	7	7
β-*β*-(Resinol)	2	3
Others	13	5

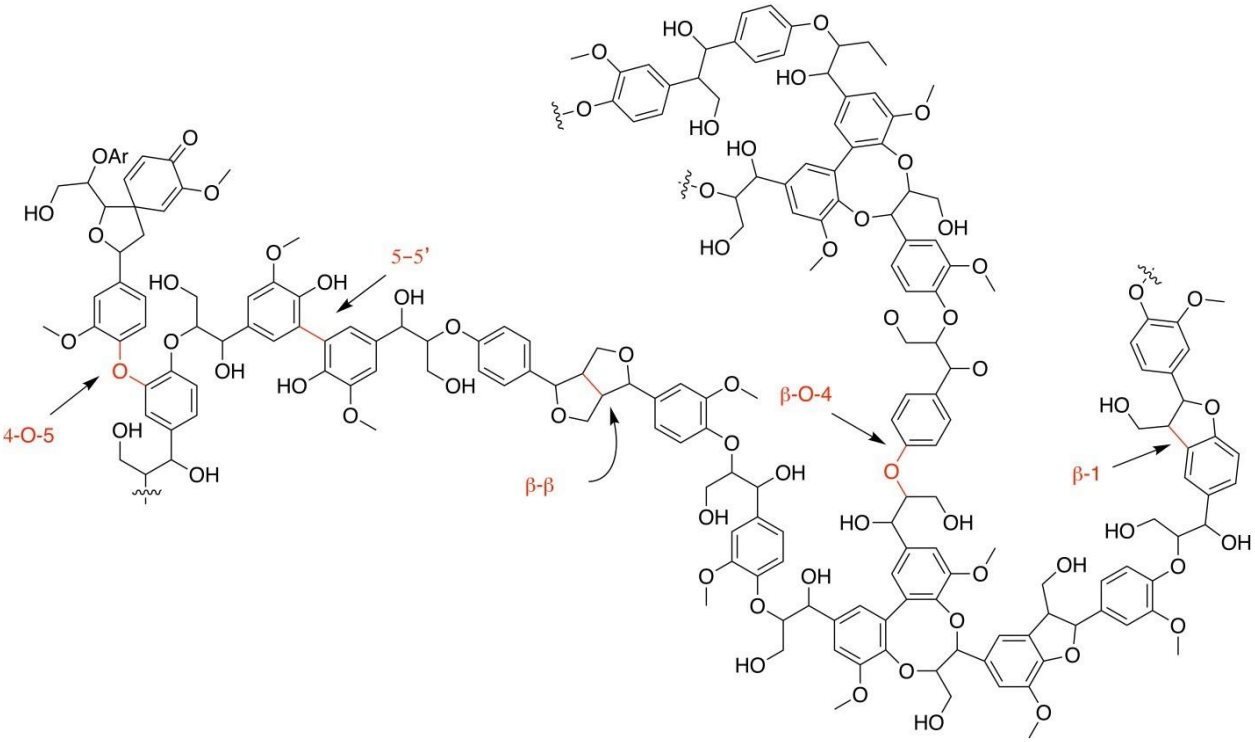

Figure 1.4: *Chemical structure of lignin with the most dominant linkages.*[15]

1.3.3. Lignin Conversion

Converting lignin into valuable chemicals is very difficult due to its complexity of structure and its physical-chemical properties like high viscosity, heat resistivity, low vapor pressure and insolubility.[9] Therefore, lignin exploitation requires advanced conversion technologies that transfer it into value added compounds. Pyrolysis is the most studied way of lignin's conversion which converts lignin to solid char, liquid oil, and gases, the proportion of which depends primarily on temperature and heating rate.[4] Hydrolysis is the process in which water is used to break down the molecules.[4] Enzymatic conversion is the bio- degradation of lignin by using enzymes produced from a living organism.[16] Multiple conversion methods and their obtainable products from lignin

and uses are provided in (Figure1.5).[4] It is worth mentioning that all of these processes are not yet at a commercial scale, but are undergoing rapid development.

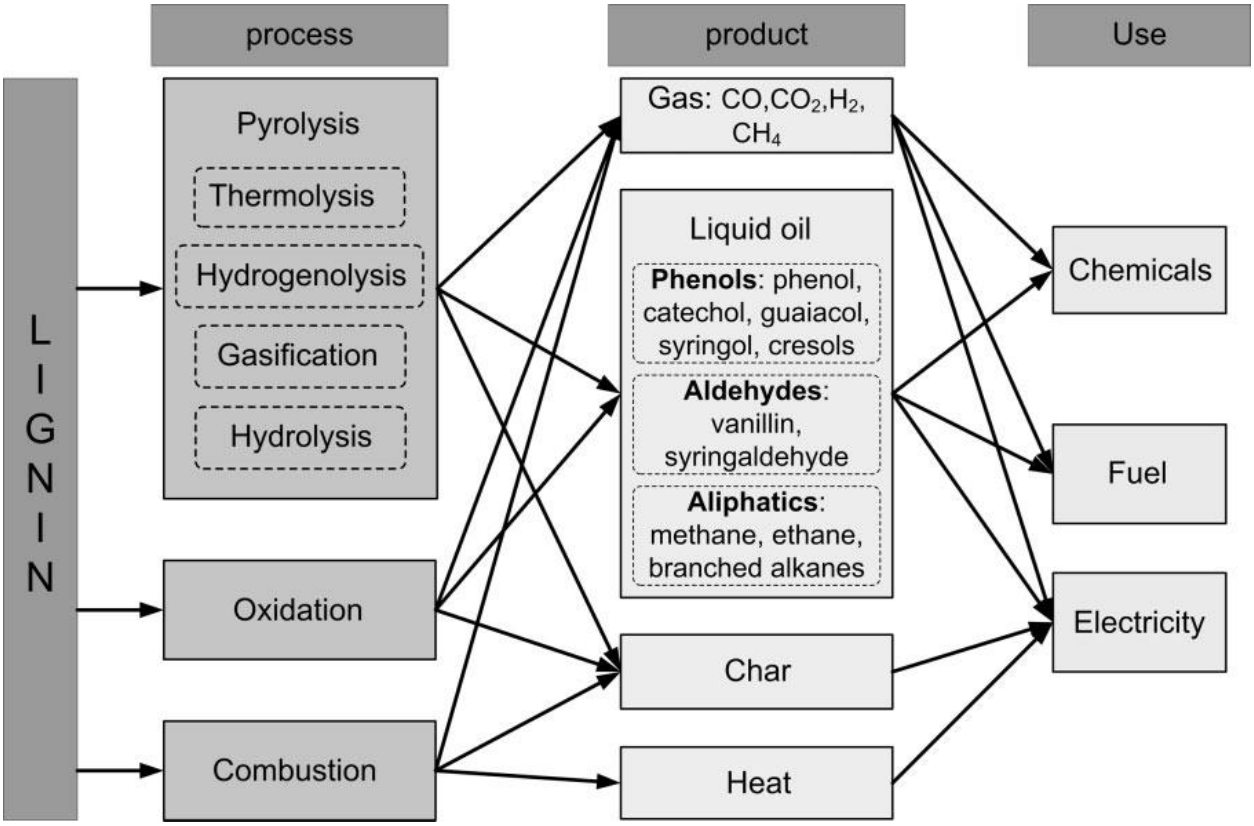

Figure 1.5: *Different conversion processes and their obtainable products from lignin with uses.*[4]

However, the separation of products is the major challenge in lignin conversion and it is costly. Therefore, catalysis seems to be the most promising method for the conversion of lignin, because the products and the catalyst can be easily separated. The catalysis approach will be discussed further in next section (1.3.3.1).

The efficiency of lignin conversion can be defined in terms of conversion factors and yield values that determine how much of the initial lignin has been successfully converted. The following equation (Eq1.1) calculates the conversion as the amount of initial lignin taking part in the reaction:

$$Conv.[wt-\%] = \frac{L_i - L_r}{L_i} 100 \qquad (Eq\ 1.1)$$

Where L_i is weight of the lignin feedstock input and L_r is the weight of the solid residue after the reaction.

There is also an alternative definition (Eq 1.2) that can be used. As follows:

$$Conv.[wt-\%] = \frac{\sum P_j}{L_i} 100 \qquad (Eq\ 1.2)$$

Where P_j is the weight of the J-th compound product.[4]

1.3.3.1. Catalysis

Catalysis has been considered an important technology in biomass and lignin conversion. Mostly, catalysts are required to assist selective bond cleavage, leading to high value compounds. Various types of catalyst have been tested for different processes and substrates including both model compounds and lignin extracts.[17] A summary of various studies is shown in (Table1.2).

Table 1.2: *A summary of various studies of catalysis regarding to conversion of lignin.*

Feedstock	Catalyst	Conversion [%]	Major Products
Oranosolv lignin	Cu/PMO[18]	100	2-Ethycylohexanol, Methylethycyclohexanol
Alkaline lignin	Zr/MCM-48[19]	49.39	Benzene, Toluene and Xylene
Phenol	Pt/HY[20]	100	Cyclohexane
Anisole	Pt/HBeta[21]	100	Benzene, Toluene and Xylene
Guaiacol	Pt/γ-Al_2O_3[22]	---	Phenol, Catechol, and 3-Methylcatechol
Guaiacol	WP/SiO_2[23]	9 - 59	Benzene, Phenol, and Methoxybenzene
4-Propylphenol	Pt/AC(N)[24]	100	Propylcyclohexane

1.4. Literature Review

Previous work involving Lignin conversion on the Pt (111) surface started with the simplest model molecules obtained from lignin; Phenol, anisole, 2-phenoxyethanol. Understanding the behavior of these simple models (mechanism, reactivity, intermediate, and products) gives insight about the reactivity of lignin. Studying lignin itself is difficult due to its high viscosity, low vapor pressure, insolubility and heat resistivity which make it hard to deal with under UHV conditions.[9,25-26] Therefore, the project started with the simple models and then we could move forward by increasing the complexity of molecules in the fragment to get much better understanding about lignin (Figure1.6).[27] In the present work, I increased the complexity of the

molecular system related to the *β-O-4* aryl ether linkage (which is the most dominant), and we focussed on di-substituted aryl species: the Veratrol family, which consists of Veratrol, 1,3-dimethoxybenzene, 1,4-dimethoxybenzene. We study the chosen molecules using surface science approaches (described in section 1.5) in order to gain insight about their reactivity. The whole family was studied via IRAS, while Veratrol was the object of an extensive study with multiple techniques: IRAS, XPS, and TPD. Surface studies of more complex molecules such as Veratrol and Guaiacol families guide understanding of the reactivity of lignin, and they will lead to the valorization of lignin.

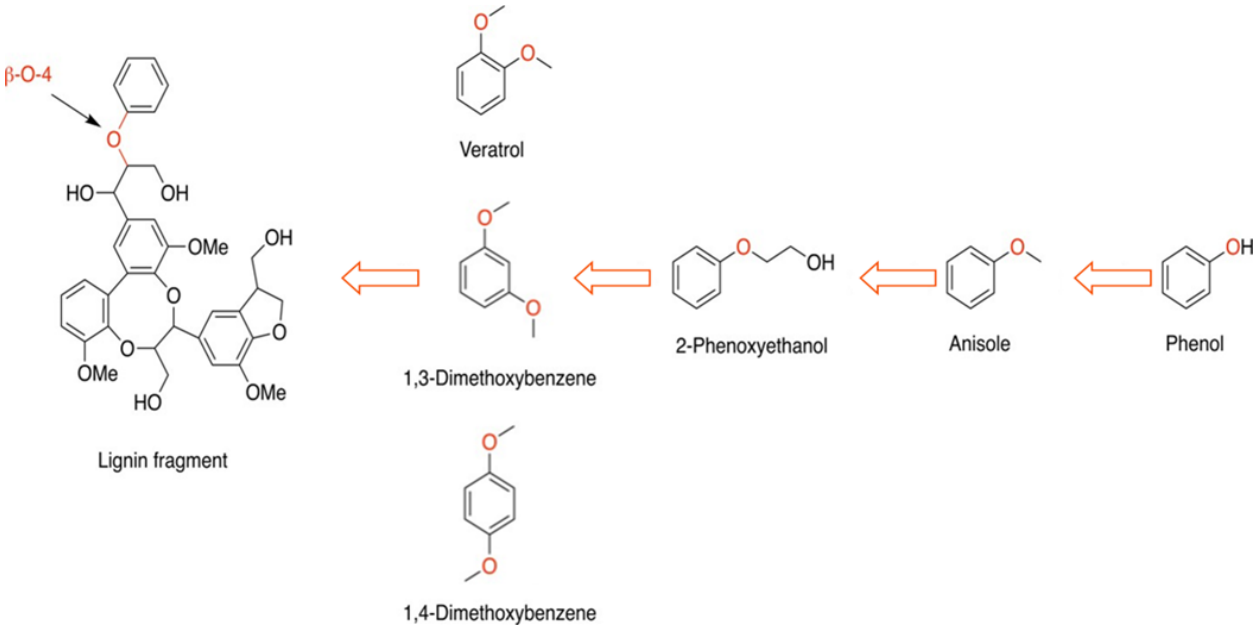

Figure 1.6: *Starting with simple lignin models and gradually increasing the complexity towards lignin. Adapted from reference.*[15]

From the work of the reactivity of phenol, anisole, and 2-phenoxyethanole on Pt (111) under ultra-high vacuum conditions, we can summarize the desorption and decomposition mechanisms as illustrated in the Figure1.7.[27] The desorption of phenol from the surface occurs in two steps: the multilayer desorbs upon reaching 220 K, and the second layer desorbs upon reaching

240 K. While the multilayer of anisole desorbs at 240 K, upon reaching 300 K, part of saturated monolayer desorbs from the surface. The 2-phenoxyethanol desorbs from the surface in two steps: the multilayer and second layer desorb from the surface upon reaching 240 K and 260 K, respectively.

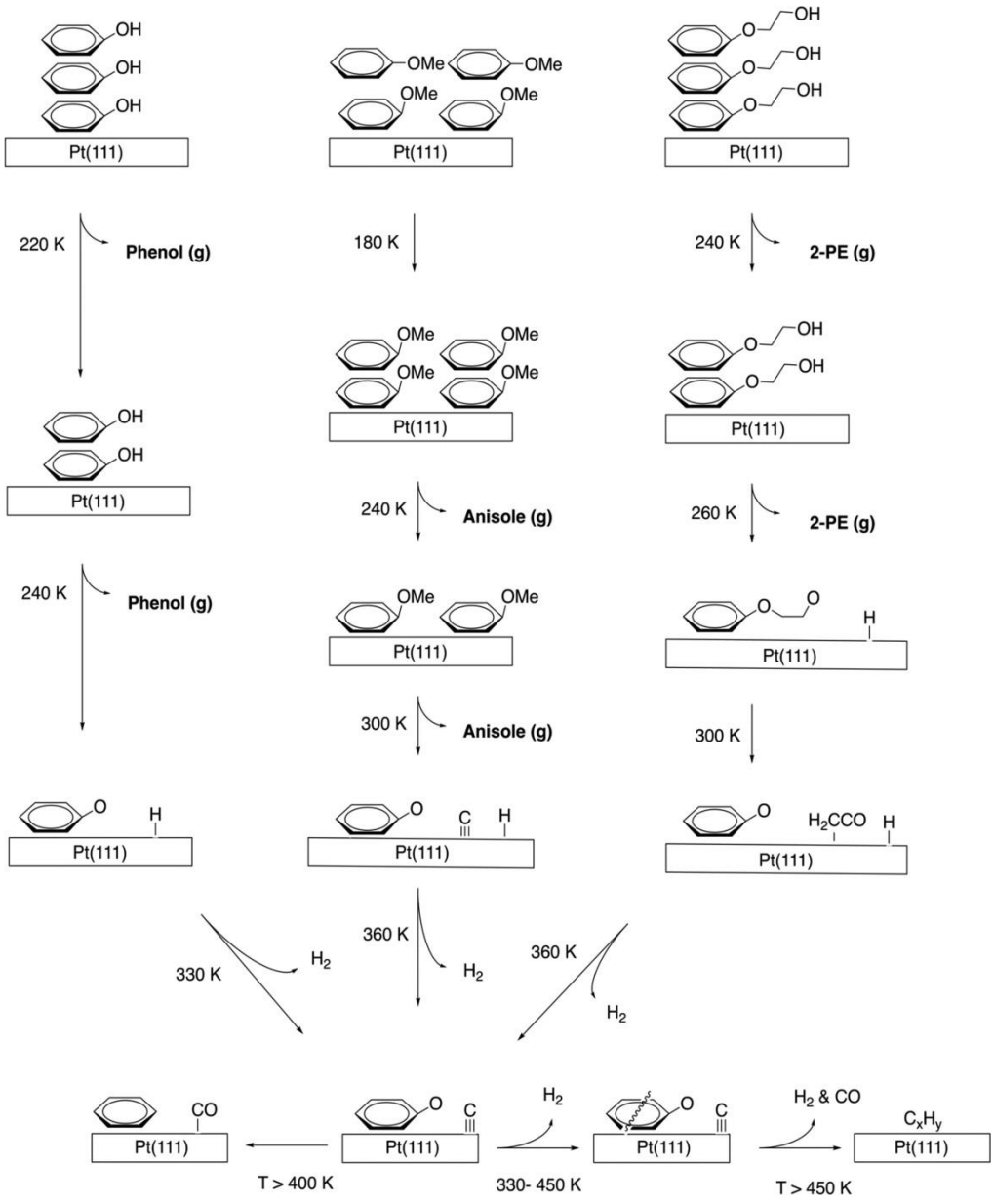

Figure 1.7: *Reaction pathways and associated temperatures for phenol, anisole, and 2-phenoxyethanol on Pt (111) under UHV conditions.*[27]

The main desorbing products of phenol are hydrogen and carbon monoxide whereas anisole desorbs four products - anisole, hydrogen, benzene, and carbon monoxide. With 2-phenoxyethanole the products are benzene, hydrogen, and carbon monoxide. The reactions take place so fast before determining which bond will cleave first, even though the DFT calculations indicate the following: for phenol O−H bond cleavage occurs below 200 K. Above 0.7 monolayer (ML) coverage phenoxy is subject to a competitive reaction pathway; it either generates benzene and surface oxygen or it decomposes into CO, H_2, and carbonaceous species. Below 0.5 ML coverage, no CH-containing adsorbates can be observed on the surface: C−C and C−H bond cleavages are more favorable than the C−O bond cleavage. For anisole, the first reaction starts with C−H bond cleavage followed by PhO−CH_2 bond cleavage (O−C) and further dehydrogenation of the methyl group to form phenoxy and carbon on the surface. For 2-phenoxyethanol, decomposition was proposed to start by O−H bond cleavage forming $PhOCH_2CH_2O$ followed by two consecutive C−H bond cleavages and then formation of phenoxy. Overall, the decomposition of all three molecules leads to the formation of phenoxy on the surface which is the key intermediate of the reactions.[9,25-26]

1.5. Approach

The approach of investigating lignin conversion in the current research involves heterogeneous catalysis by choosing a single crystal as catalyst and dosing molecules in gas phase through a UHV system. The main techniques are IRAS, XPS, and TPD. This section highlights the approach concepts.

1.5.1. Heterogeneous Catalysis

The preferred method for conversion of lignin is heterogeneous catalysis due to its ability to accelerate the reaction and allow for separation of products.[28-29] The catalytic process works to reduce the activation energy of selected reactions, guiding product selectivity.[9,28,30] This makes biomass conversion viable. Plus, heterogeneouscatalysis is the best method to separate products from the catalyst surface, which is quite challenging and costly in other conversion methods like pyrolysis and hydrothermal.[15] In our case, the system of heterogonous reactions is in gas/solid phases, and the reactions occur at the interface between these phases.[29] Commercial heterogeneous catalysis is performed via nanostructured materials. Here we use a single crystal to simplify and be able to interpret/identify key processes. Same for pressure, commercial is room or high pressure, here is UHV.

1.5.2. Pt (111) Model Catalyst

Choosing the surface plays an essential role in heterogeneous catalysis for understanding the interactions of lignin with the catalyst on the molecular level. The single crystal is well defined surface which makes the determination of the molecules easier.[29] The <111> orientation is thermodynamically stable and also very reactive surface.[29] The previous studies showed (Table1.2) the platinum surface is very promising catalyst in terms of high conversion rates and selectivity in

the valorization of lignin.[20,21,24] The Pt (111) single crystal used in this study has the shape of 8 mm diameter and 0.5 mm thick with purity 99.99%.

1.5.3. Ultra-high Vacuum

The most required condition in surface science approaches is maintaining a well-characterized surface since we are probing interfaces at the molecular level. Moreover, a clean environment at the atomic level is a significant factor to avoid the interferences of surrounding particles.[29] The ultra-high vacuum (UHV) in the range of $1x10^{-10}$ mbar is the key part to create an isolated system in order to probe the interaction of the molecule on the catalyst surface without any interference of the surrounding environment, and UHV system keeps the catalyst clean and allows for recleaning if needed (Figure 1.8).[29] The need of UHV system in surface science approaches will be discussed further in Chapter II.

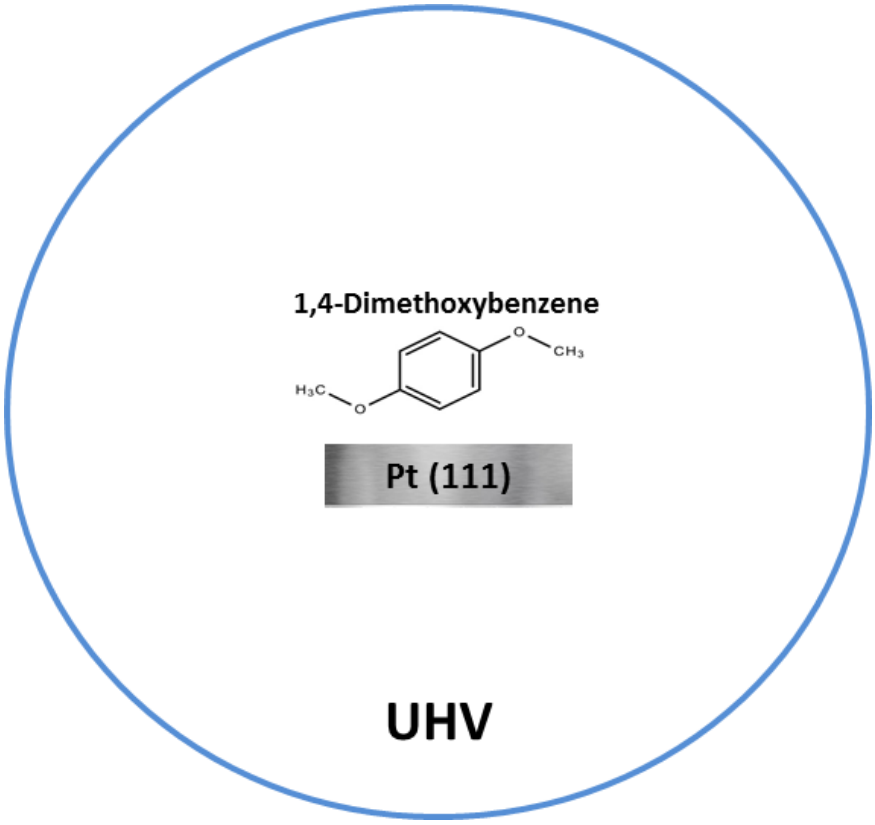

Figure 1.8: *An investigation of 1,4-dimethoxybenzene in gas phase on a solid single crystal Pt (111) under UVH conditions. Adapted from reference.*[15]

1.5.4. Instrumentation

The main probe technique in this thesis is Infrared Reflection-Adsorption Spectroscopy (IRAS) that provides valuable information about the adsorption geometry, and the intermediate species of the decomposition. Also, additional two techniques are involved into the present work, X-ray Photoelectron Spectroscopy (XPS) measures the elemental of the model molecules on the solid surface, and Temperature programmed desorption (TPD) to study the molecule desorption by programmed heating. All of the techniques are under the UHV conditions.

References:

(1) Hans-Wilhelm Schiffer. *World Energy Resources | 2016*; the World Energy Council: London, **2016**.

(2) CIA World Factbook. **2015** https://www.cia.gov/library/publications/the-world-factbook/geos/xx.html.

(3) Goldemberg, J. Ethanol for a Sustainable. *Science (80-.).* **2007**, *315*, 808–8010.

(4) Pandey, M. P.; Kim, C. S. Lignin Depolymerization and Conversion: A Review of Thermochemical Methods. *Chem. Eng. Technol.* **2011**, *34*, 29–40.

(5) Mehmood, S.; Anwar, Z.; Shahzadi, T.; Sughra, K.; Rashid, U.; Afroz, A.; Irshad, M.; Zeeshan, N. Advances in Lignocellulosic Biotechnology: A Brief Review on Lignocellulosic Biomass and Cellulases. *Adv. Biosci. Biotechnol.* **2014**, *5*, 246–251.

(6) Kulkarni, P.; Lavanya, D.; Dixit, M.; Kanth Raavi, P.; Vamsi Krishna, Ln. Sources of Cellulose and Their Applications – A Review. *Int. J. Drug Formul. Res.* **2011**, *2* (6), 28–32.

(7) Ma, R.; Pekarovicova, A.; Fleming, P. D.; Husovska, V. Preparation and Characterization of Hemicellulose-Based Printable Films. *Cellul. Chem. Technol.* **2017**, *51* (9), 939–948.

(8) Hansen, N. M. L.; Plackett, D. Sustainable Films and Coatings from Hemicelluloses: A Review. *Biomacromolecules* **2008**, *9*, 1493–1495.

(9) Reócreux, R.; Ould Hamou, C. A.; Michel, C.; Giorgi, J. B.; Sautet, P. Decomposition Mechanism of Anisole on Pt(111): Combining Single-Crystal Experiments and First-Principles Calculations. *ACS Catal.* **2016**, *6*, 8166−8178.

(10) Haghdan, S.; Renneckar, S.; Smith, G. D. Sources of Lignin. In *Lignin in Polymer Composites*; **2015**.

(11) Santos, R. B.; Capanema, E. A.; Balakshin, M. Y.; Chang, H. M.; Jameel, H. Lignin Structural Variation in Hardwood Species. *J. Agric. Food Chem.* **2012**, *60*, 4923−4930.

(12) Pepper, I. L.; Gerba, C. P.; Gentry, T. J. *Environmental Microbiology*; Elsevier, **2015**.

(13) Eero Sjöström. *Wood Chemistry Fundamentals and Applications, Second Edition*, 2nd ed.; Elsevier Inc, **1993**.

(14) De Araujo, F.; Hart, J. F.; Mansfield, S. D. Variation in Trembling Aspen and White Spruce Wood Quality Grown in Mixed and Single Species Stands in the Boreal Mixedwood Forest. *Forests* **2015**, *6* (5), 1628–1648.

(15) Cherif A. Ould Hamou. Decomposition Mechanism of Lignin Models on Pt(111) : Combining Single Crystal Experiments and First Principle Calculations, University of Ottawa, **2019**.

(16) Bugg, T. D. H.; Rahmanpour, R. Enzymatic Conversion of Lignin into Renewable Chemicals. *Curr. Opin. Chem. Biol.* **2015**, *29*, 10–17.

(17) Gabor A. Somorjai; Yimin Li. *Introduction to Surface Chemistry and Catalysis*, 2nd ed.; Wiley, **2010**.

(18) Barta, K.; Matson, T. D.; Fettig, M. L.; Scott, S. L.; Iretskii, A. V.; Ford, P. C. Catalytic Disassembly of an Organosolv Lignin via Hydrogen Transfer from Supercritical Methanol. *Green Chem.* **2010**, *12*, 1640–1647.

(19) Elfadly, A. M.; Zeid, I. F.; Yehia, F. Z.; Abouelela, M. M.; Rabie, A. M. Production of Aromatic Hydrocarbons from Catalytic Pyrolysis of Lignin over Acid-Activated Bentonite Clay. *Fuel Process. Technol.* **2017**, *163*, 1–7.

(20) Hong, D. Y.; Miller, S. J.; Agrawal, P. K.; Jones, C. W. Hydrodeoxygenation and Coupling of Aqueous Phenolics over Bifunctional Zeolite-Supported Metal Catalysts. *Chem. Commun.* **2010**, *46*, 1038–1040.

(21) Zhu, X.; Lobban, L. L.; Mallinson, R. G.; Resasco, D. E. Bifunctional Transalkylation and Hydrodeoxygenation of Anisole over a Pt/HBeta Catalyst. *J. Catal.* **2011**, *281*, 21–29.

(22) Nimmanwudipong, T.; Runnebaum, R. C.; Block, D. E.; Gates, B. C. Catalytic Conversion of Guaiacol Catalyzed by Platinum Supported on Alumina: Reaction Network

Including Hydrodeoxygenation Reactions. *Energy and Fuels* **2011**, *25*, 3417–3427.

(23) Zhao, H. Y.; Li, D.; Bui, P.; Oyama, S. T. Hydrodeoxygenation of Guaiacol as Model Compound for Pyrolysis Oil on Transition Metal Phosphide Hydroprocessing Catalysts. *Appl. Catal. A Gen.* **2011**, *391*, 305–310.

(24) Ohta, H.; Kobayashi, H.; Hara, K.; Fukuoka, A. Hydrodeoxygenation of Phenols as Lignin Models under Acid-Free Conditions with Carbon-Supported Platinum Catalysts. *Chem. Commun.* **2011**, *47*, 12209–12211.

(25) Ould Hamou, C. A.; Réocreux, R.; Sautet, P.; Michel, C.; Giorgi, J. B. Adsorption and Decomposition of a Lignin β-O-4 Linkage Model, 2-Phenoxyethanol, on Pt(111): Combination of Experiments and First-Principles Calculations. *J. Phys. Chem. C* **2017**, *121*, 9889−9900.

(26) Ihm, H.; White, J. M. Stepwise Dissociation of Thermally Activated Phenol on Pt(111). *J. Phys. Chem. B* **2002**, *104*, 6202–6211.

(27) Ould Hamou, C. A.; Giorgi, J. B. Direct Observation of Phenoxy as the Key and Common Intermediate for the Decomposition of Lignin Fragments Containing the β-O-4 Linkage. *J. Phys. Chem. C* **2018**, *123 (13)*, 8122-8132.

(28) Nørskov, J. K.; Studt, F.; Abild-Pedersen, F.; Bligaard, T. *Fundamental Concepts in Heterogeneous Catalysis*; **2014**.

(29) Kurt Kolasinski, D. W. *Surface Science: Foundations of Catalysis and Nanoscience Second Edition*, 2nd ed.; John Wiley & Sons, Ltd, **2008**.

(30) Boucher-Jacobs, C.; Nicholas, K. M. *Selective Catalysis for Renewable Feedstocks and Chemicals*; Springer, **2014**.

Chapter 2

Techniques and Experimental Setup

Chapter 2: Techniques and Experimental Setup.

2.0. Experimental

This chapter illustrates the experimental techniques of this thesis, theoretically and practically. Since all experiments were performed in ultra-high-vacuum (UHV), I will introduce the environment and how to achieve it. The main technique of my research is infrared reflection absorption spectroscopy, IRAS, and therefore this technique will be discussed in detail. Also the common surface science techniques that relate to this thesis, X-ray Photoelectric Spectroscopy (XPS) and Temperature Programmed Desorption (TPD), will be discussed in this chapter.

2.1. Ultra-High Vacuum

All the experiments and techniques in the present work are performed in UHV conditions. The equipment is designed to achieve Ultra High Vacuum (pressure reaches 1×10^{-10} mbar) using advanced technology in both vacuum pumps and pressure gauges. The UHV techniques started in the early 1960s when the first Ultra High Vacuum system was achieved.[1] A number of techniques used initially for fundamental studies have since been developed into advanced and widely used methods for routine surface analysis. As technology advances, viable new techniques are still being invented and established methods are still being improved at, like the IRAS which is the main technique of this work.[2]

The UHV in the IRAS's Chamber is achieved by a combination of a turbomolecular pump and a mechanical pump. The turbomolecular pump is able to reach pressures below $1x10^{-8}$ mbar before baking, while the mechanical pump provides $1x10^{-2}$ mbar backing the turbomolecular pump. Two differentially pumped windows required to allow the infrared beam to cross the chamber are mounted on opposite sides of the UHV chamber. These windows have 2.75" CF

flanges and use KBr 38 x 6mm optical crystals with a 1/4" tube for differential pumping. Fluorocarbon O-rings are used as seals between the chamber and the windows. The entire optical pathway outside UHV is purged with dry air. Great care should be taken during the manipulation of the components because all the tools in the chamber are delicate and not easily replaced. The replacement of anything inside the chamber requires opening the chamber, which means losing the UHV and necessitating re-achievement of the UHV by "baking out" the whole chamber.

"Baking out" the chamber means heating the walls of the chamber to ~100 C in order to degas the molecules that stick to the walls inside the chamber to achieve UHV. Degassing the molecules allows the pressure in the chamber to decrease below 10^{-8} mbar while the pumps are running. The baking of the IRAS's chamber is done by wrapping a heating tape on the chamber and connecting it with a voltage source (≈80 volt) as shown in (Figure 2.1.A). Then, the whole chamber is covered by aluminum foil, as shown in (Figure 2.1.B). The foil reflects the thermal energy back to the Chamber's walls. The efficient baking out process takes about 24-92 hours. The pumping system alone is unable to remove the molecules from the chamber's walls without taking a very long time; baking accelerates the process.[3]

Figure 2.1*: (A) Illustration of how to wrap the heating tape. (B) Covering the stainless steel with foil.*

2.2. The need for UHV

The surface science approach involves probing interfaces at the molecular level, and describes the reactions and properties at this level. Providing an environment in which a completely clean sample surface can be maintained in a cleaned state over time is necessary for experiments.[1] Also, it is necessary to reduce the number of molecules in the chamber to a point where the gas density is low enough to permit experiments involving electrons and ions traveling distances without interference from gas phase scattering.[1] The impingement rate, which is the number of particles that hit a surface per second striking a unit area, is dependent on the pressure as given by the Hertz-Knudsen equation:

$$Z_W = \frac{P}{(2\pi m k_B T)^{\frac{1}{2}}} \quad (Eq\ 2.1)$$

Clearly, the rates of impingement will decrease with decreasing pressure. Also, there are other parameters that need to be taken in account: the sticking coefficients and residence time. If one assumes at 300K, for a gas with the mass of N_2, and the atomic density of a solid surface is $1x10^{15}$ in a monolayer.[1] By using the values in equation (Eq 2.1) we get this:

$$Z_W = (\ 3.8x10^5 MLS^{-1})P \quad (Eq\ 2.2)$$

Thus, at pressure around $1x10^{-6}$ torr, the number of molecules that hit the surface is roughly equal to one monolayer.[1] On average, every surface atom is struck by at least one molecule from the gas phase every second. Now, if each of these molecules stuck to the surface and adsorbed, the surface would be completely covered in only 1 second. Therefore, in order to keep the surface clean, or to keep a specifically covered surface unaltered by further adsorption for the time it takes to run an experiment, for instance one hour, then the pressure needs to remain lower, at least:

$$\left(\frac{1X10^{-6}}{3600}\right) = 2.77X10^{-10}torr \quad (Eq\ 2.3)$$

So, the use of an ultrahigh vacuum is a necessity to maintain those surfaces in a contamination-free state for the duration of the experiment.[1]

The mean free path, which is the distance that the particles travel on average between collisions depends on the pressure as well, but inversely. In an ideal gas, with a collision frequency Z and mean velocity $\bar{\upsilon}$, its value is given by:

$$\lambda = \frac{\bar{\upsilon}}{Z} = \frac{k_B T}{\sqrt{2}\sigma P} \quad (Eq\ 2.4)$$

Assuming, the collision cross section of N_2 is $\sigma = 0.43$ nm^2, at a pressure of P = 1 atm = 760 torr, the mean free path would be just 70 nm; while at P=1.3x10^{-13} atm =1x10^{-10} torr, the mean free path is over 450 km. This means the particle will travel a distance 450 km before a collision occurs. In electron spectroscopy, the ultrahigh vacuum is required in order to maintain a large mean free path for the electrons and ions to avoid collisions and scattering events that would result in loss of the electrons' kinetic energy.[1]

2.3 Sample Preparation

Sample preparation consists of a number of sputtering-annealing cycles as discussed in the experimental sections of chapters 3 and 4. The preparation uses a number of elements/devices described below.

2.3.1 Sample Holder

The sample holder is used to manipulate the sample and it holds heating elements and thermocouples used to control the cleaning cycle. The design of the sample holder in our setup is

a “Z” shaped molybdenum plate; (Figure 2.2). The reason for the “Z” shape is to allow an incidence angle of the IR beam between 2-10^0 on the sample (limited by the geometric limitations of the chamber). The sample holder is mounted on the end of the manipulator, allowing for a 500 mm linear transfer of the sample holder in the z direction, with a 360° rotational range. The sample’s position has to be very close to the reservoir in order to be able to achieve the lowest temperature possible (down to 110K). The manipulator is also mounted on an x-y stage, which allows the arm to move within a 25 mm range in the x and y directions. The holder is made of molybdenum material because of its low vapor pressure, high melting point, low thermal expansion, hardness, and high resistance to corrosive chemicals.

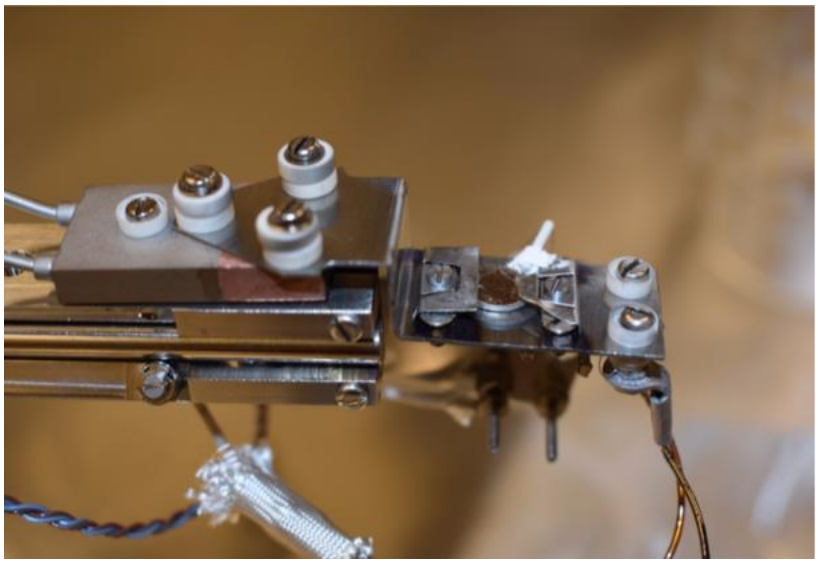

Figure 2.2: *A photograph of the sample holder of the IRAS. The photo is taken from the Giorgi Lab photography database.*

2.3.2 Thermocouples

The heating and the cooling in the system need to be measured. Thermocouples are used for this purpose. The thermocouples used in our setup are K-type, which have a range of -200 – 1350 C^0. K-type thermocouples are made of Chromel and Alumel.[4] The principle of the thermocouples is measuring the voltage at the junction of the two metals.[4] The changing of the voltage depends on the temperature at the junction and is calibrated, so the temperature can be directly measured. The junction must be on the sample to measure the temperature of the sample accurately.[4]

2.3.3 Sputtering

The surface, due to continually use, becomes covered with a layer of atoms or molecules. So, it is mandatory to clean the surface before running the experiment. Sputtering is the best way to clean the surface of the catalyst. Sputtering is shooting high energy particles onto the surface in order to remove the atoms from the surface.[5] The sputtering gun used in this setup is the Specs IQEH-A model. It is operated in the range of 1.5 KeV kinetic energy and uses Argon ions with 99.999% purity as gas source. The sputtering is run with the sample at a high temperature, 600K, with a pressure of $1x10^{-5}$ mbar with repetitive cycles of 30 minutes each, ideally, three cycles are followed by annealing.

2.3.4 Annealing

Annealing is the ability to reach a very high temperature--about 1200K on the sample. By providing enough energy, atoms will be allowed enough mobility on the sample surface to achieve an optimal surface orientation.[6] Annealing also will help to desorb the unwanted atoms from the surface. The annealing follows the sputtering cycles, heating to 1100 K for 2 minutes at UHV pressure.

2.4. Infrared Reflection-Adsorption Spectroscopy (IRAS)

This section will discuss further the main instrument of the present research. It starts with an introduction and a historical background of the technique. Then, it will delve into the principles behind the IRAS, and its major components. Lastly, the advantages and disadvantages of the infrared reflection-adsorption spectroscopy will be covered.

2.4.1. An Introduction and Historical Background

Infrared reflection-adsorption spectroscopy is a vibrational spectroscopic technique used commonly in surface science approaches to study submonolayer films adsorbed on reflective substrates such as a metal (Platinum in this approach).[7] Nowadays, the most suitable technique to study catalytically relevant adsorption systems on such surfaces is IRAS, comparing with other surface techniques such as Raman Spectroscopy and High-Resolution Electron Energy Loss.[8] The method also has different acronyms, such as RAIRS, FT-IRAS, IRRAS, and ERIRS (external reflection infrared spectroscopy). All of these names refer to the same principle of measurement which basically uses IR radiation and reflection adsorption geometry.[9]

The history of infrared reflection adsorption spectroscopy began in the late 1960s, when the first application of the technique was performed.[7] But, the full history has to be begin in 1880 when Michelson discovered his interferometer. Only by knowing where FTIR has come from can it be understood where it is today.[10] The Michelson interferometer was not originally designed to perform infrared spectroscopy. However, Dr. Michelson was aware of the potential use of the interferometer to obtain spectra, and measured many interferograms manually. The time required to convert the interferograms into spectra made using the interferometer to obtain spectra unwieldly. J.W. Cooley and J.W. Tukey invented the fast Fourier-Transform (FFT) which made Fourier-transform infrared spectroscopy possible in the middle of the 1960s.[10]

Applications of infrared spectroscopy started in the late 1930s, and became well-established by the characterization of supported catalysis in the 1960s.[7] The early studies used powdered or porous substrates with a high specific area (between 1- 1000 m^2/g) that allowed milligram quantities of the adsorbed species to be introduced into the infrared beam.[7] The 1960s witnessed a lot of developments for a range of surface science probes capable of determining adsorbate structures and electronic energy levels on single-crystal and other well-defined substrates. At the end of the decade, the first characterization of an adsorbate on a single-crystal substrate was achieved in Pritchard's laboratory. This group pioneered the integration of IRAS with other techniques of surface science.[7] Until the middle 1980s, IRAS was mainly confined to studying the C-O stretch vibration of chemisorbed carbon monoxide. Around that time, most IRAS studies were performed with dispersive spectrometers which were based on diffraction gratings poorly suited to the rapid scanning of broad ranges of the infrared spectrum.[7] At the end of the decade, all studies virtually employed a commercial FTIR in the IRAS technique. Chesters was the first to describe results from FTIR based on an IRAS setup, which gave a clear advantage over the dispersive spectrometers.[11] Since then, many developments have been made to the IRAS technique in order to improve its performance, such as the optimizing of the signal-to-noise ratio and the optical configuration.

2.4.2 The Principle of IRAS

Reflection-absorption infrared spectroscopy is basically an FTIR coupling with a UHV Chamber, where the IR beam is specularly incident on a grazing angle of adsorbed molecules on well-defined solid surface like Pt (111) with a high sensitivity (typically 0.1% of a CO monolayer). The technique provides important information about the adsorption geometry and the integrity of the adsorbed molecules by creating the possibility for a systematic determination and assignments of vibrational features in molecular species adsorbed on the single crystal surface. The principle of IRAS is to excite the vibrational modes of the absorbent by emitting infrared radiation on the surface. As Figure 2.3 shows, the IR beam emitted from the FTIR (Bruker Equinox 55) is directed by a flat mirror that reflects the beam at 90^0 to the parabolic mirror (f=30 cm , 90^0 off-axis), which focuses the beam on the sample's surface inside the UHV chamber with an angle of incidence of 7^0. The IR beam gets reflected from the surface, but the IR light will be absorbed by the molecules when the incident IR light matches its vibrational frequencies. After the reflection from the surface, the reflected beam is collected by the second parabolic mirror and then the beam is refocused onto the MCT detector.

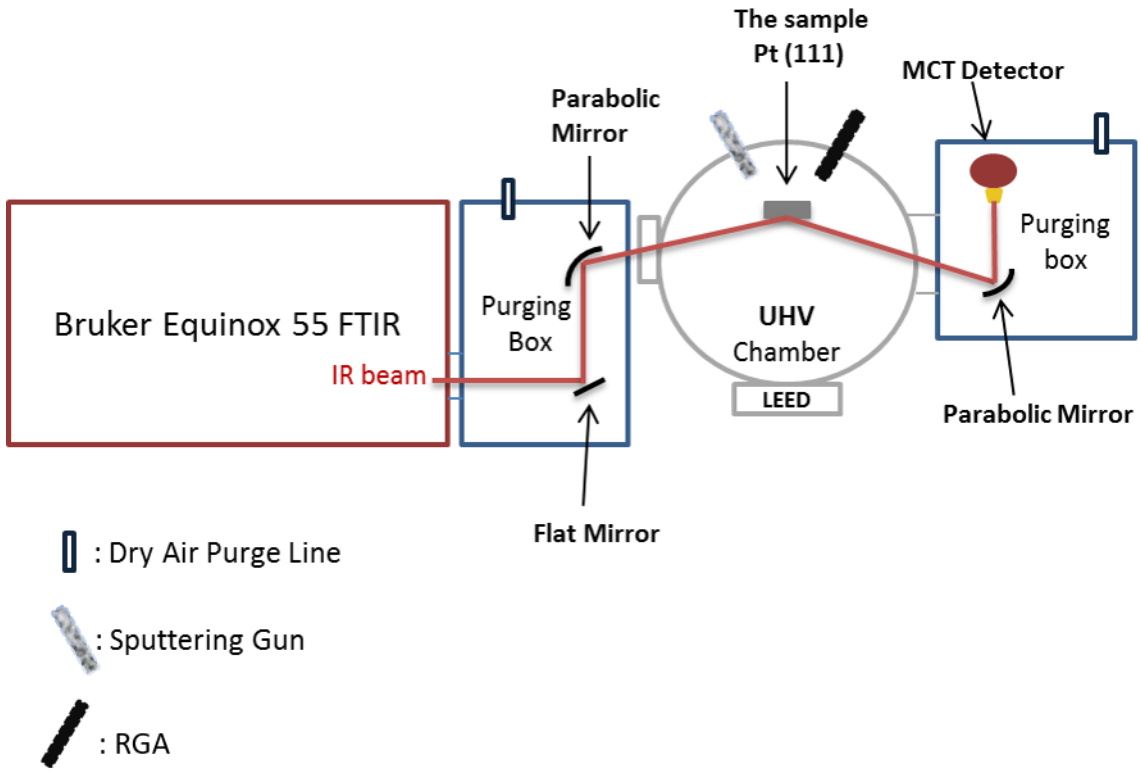

***Figure 2.3**: Schematic diagram of the IRAS system setup with its components.*

The absorbed frequencies can be determined by measuring the reflected IR beam. Each molecule has its own vibrational modes because the frequency at which a given vibration occurs depends on the strength of the bond and the mass of the atoms. Thus, the technique will provide valuable information about the chemical structure of the molecule.

The vibration of a molecule in the gas phase gets excited by the interaction of the electric field of incident IR light with the dipole moment of the molecule. So, let's zoom in at the surface in order to understand the absorption process of incident light on the absorbent, (Figure 2.4).

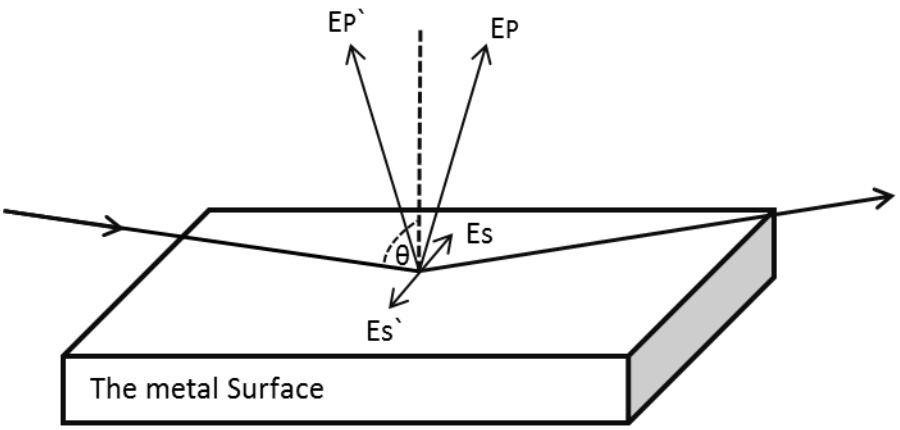

Figure 2.4: *Electric fields of s-and p-polarized radiation incident on a metal surface at an angle θ to the normal. Primed and unprimed vectors refer to the reflected and incident beams respectively.*

The electric field of the incident light has two components; $\boldsymbol{E_s}$ is the electric field incident to the surface with a parallel polarization, and $\boldsymbol{E_p}$ which is the electric field that incident with a perpendicular polarization to the surface. Also, $\boldsymbol{E_{s'}}$ is the reflected electric field with a parallel polarization, and $\boldsymbol{E_{p'}}$ is reflected electric field with a perpendicular polarization.[7] The electric fields $\boldsymbol{E_s}$ and $\boldsymbol{E_{s'}}$ are hence almost exactly equal and opposite, and therefore they cancel each other. The $\boldsymbol{E_p}$ and $\boldsymbol{E_{p'}}$ get enhancement and interact with the perpendicular dipoles moment of the molecule due to the metal surface selection rule.[7]

2.4.3. The Components

The technique is integrated by three main components: the IR source; the FTIR optics; and, the MCT detector. This section will focus on these components.

2.4.3.1. The Infrared Source

The infrared source used in FTIR (Equinox 55) is a globar, which is a solid light source made of silicon carbide. The fundamental principle depends on black body radiation. The globar is heated by the resistor heating method via a current source. The silicon carbide rod is heated to a

temperature up to 1200 K because the intensity of the black body radiation mainly depends on the temperature. It then combines with a downstream interference filter to produce a radiation having wavelengths of (2.5-25μm).

2.4.3.2. Fourier Transform Infrared Spectroscopy

The Fourier transform infrared spectroscopy is the major component of the IRAS, which contains a Michelson Interferometer. The purpose of using the interferometer is to measure the wavelength of IR beam by creating interference patterns. The Michelson interferometer contains a beam splitter, fixed mirror, and a movable mirror as illustrated (Figure 2.5).[8]

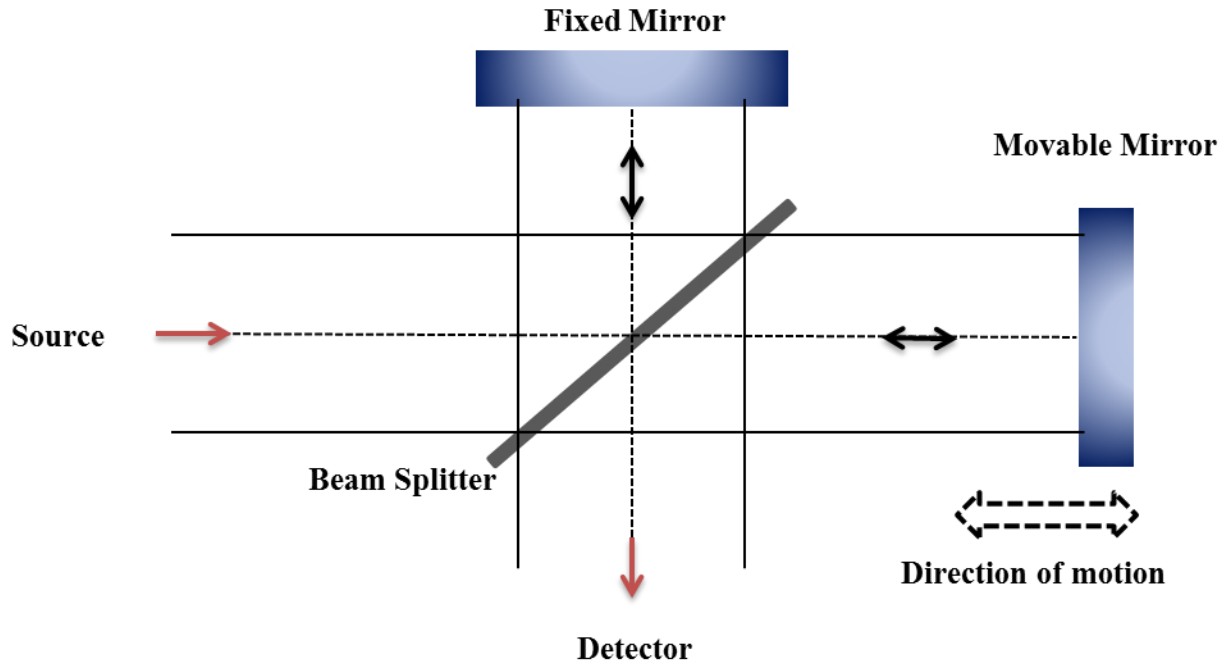

Figure 2.5: *Schematic representation of the Michelson interferometer. Adapted from reference.*[8]

The IR beam initiates from the source to the beam splitter, which divides the input beam into two beams, partially reflected to the fixed mirror, and partially transmitted to the movable mirror. The movable mirror moves continuously back and forth along an axis perpendicular to its plane as

shown in the (Figure 2.5). The two beams are recombined again after they are reflected back to the beam splitter and then they interfere, partially reflected and partially transmitted. Because of the effect of interference, the intensity of each beam, one passing to the detector and the other returning to the source, depends on the difference of path lengths in the two arms of the interferometer, which is known as optical path difference or optical retardation (δ).[12] This is important to understand because after the recombination of the beam on the other side of the beam splitter the beam will form an image on the detector. The intensity of the composite beam depends very strongly on the optical path difference (δ).[8] In fact, the composite beam is an interference pattern. The variation in the intensity of the beams detected by the detector is a function of the optical path difference (δ) and the graph is plotted with this intensity versus mirror position (cm) which is known as an interferogram I (δ), (Figure 2.6). If the optical path difference (δ) is zero, where both mirrors have the same distance from the beam splitter, then constructive interference occurs.[12] Other values of the (δ) will be a partially or totally destructive interference appears. When a mathematical function known as the Fourier-transform is applied to the interferogram a single beam spectrum of intensity I versus wavenumber W (cm^{-1}) is obtained. This transformation is expressed mathematically as:

$$I(W) = \int_{-\infty}^{+\infty} I(\delta) \cos(2\pi W\delta)\, d\delta \qquad (Eq\ 2.5)$$

The Fourier transform converts the I (δ) information to an I (W) plot of intensity versus wavenumber. These processes are done by computational software called OPUS. Thus, for transmission measurements, there are two spectra which must be acquired: first spectrum is acquired before dosing a molecule on the clean Pt (111) surface. This is known as the single beam reference (SBR) or I_0 spectrum. The single beam reference always has peaks of the artifacts of the

environment in the UHV chamber such as vapor water and carbon dioxide. The second spectrum is acquired after dosing a certain amount of the molecule being tested, which contains peaks of the absorption molecule. This spectrum is called the single beam sample (SBS) or I spectrum. Therefore, by dividing the I by I_0 the transmittance spectrum will be obtained as shown in (Figure 2.6).

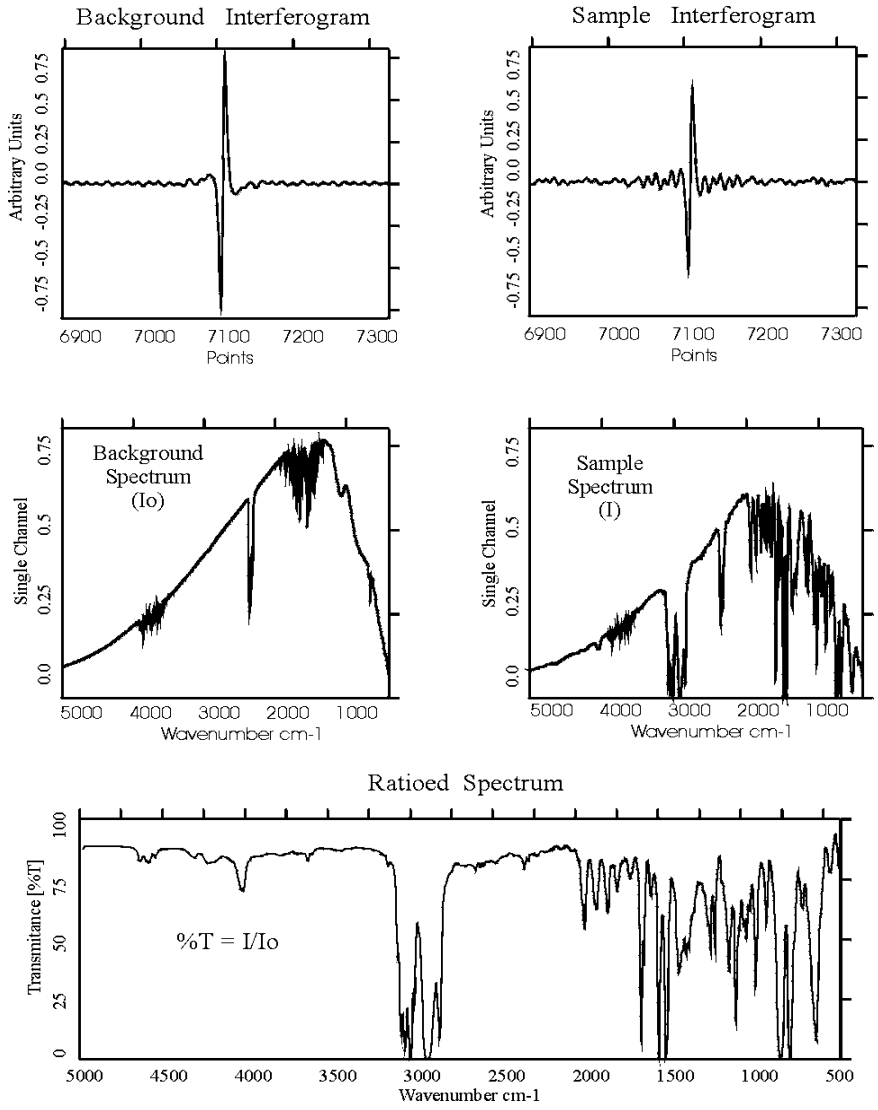

Figure 2.6: *Two interferograms are recorded, each of these is Fourier transformed to produce single beam spectra $I_\circ$ and I respectively. Transmittance spectrum is obtained by dividing I by $I_\circ$.*[12]

2.3.3.3 The MCT Detector

The Mercury-Cadmium-Telluride (MCT) detector (Infrared associates, model D315/6) is the last optical tool that receives the IR beam after the reflection from the sample's surface . It transfers it to the computer after it is translated by Fourier Transform equations. The MCT detector used in the IRAS consists of a crystal made of three elements: a thallium bromoiodide (KRS-5W) window to protect the crystal, a reservoir of liquid nitrogen to cool down the detector; and, electronics to measure the current. This model is able to detect wavelengths between 2-24 μm with a peak at 22 μm (λ_{max}) due to its sensitivity to the infrared light. When the infrared light interacts with the crystals, electrons from the valance band are excited to the conduction band. By applying the voltage, the current can be measured, and it is proportional to the number of photons hitting the detector. Therefore, the measured current gives the measure of infrared intensity. The reason for the cooling down by liquid nitrogen is to avoid the excitation of the electrons which might occur because of thermal agitation; this will decrease the level of noise.

2.4.4. The Advantages and Limitations

Like any other technique, the IRAS has a lot of distinctive advantages over many vibrational surface science instruments, but also it has some limitations. This section will provide the primary advantages and disadvantages of the IRAS.

2.4.4.1. The Advantages

The high resolution around 1 cm^{-1} and high sensitivity (0.1% of a CO monolayer) are some of the advantages of IRAS over other surface science techniques such as high-resolution electron energy loss (HREELS) and Raman Spectroscopy. Also, the IRAS can be employed on a variety of surfaces, single crystal and complex real catalysts, under the UHV conditions.[8]

An advantage of this technique which is particularly to the FTIR is that the FTIR can acquire a spectrum much faster than the dispersive instrument (an instrument does the same job of FTIR).[10] This allows multiple scans of the same sample to be added together. The signal-to-noise ratio for constant resolution is related to the number of scans added together as follows:

$$SNR \propto (N)^{\frac{1}{2}} \quad (Eq\ 2.6)$$

N is the number of scans added together. As an example, a single 4 cm^{-1} resolution scan from 4000-400 cm^{-1} on the dispersive instrument takes about 10 minutes.[10] The same spectrum on the FITR takes only one second. This means the FTIR can obtain 600 scans in 10 minutes. As a result, the FTIR can achieve a signal-to-noise ratio advantage of $(600)^{1/2}$ a factor of (24.5) versus the dispersive instrument in the same amount of time. For this reason, the FTIR currently replaces the dispersive instrument and becomes the instrument of choice for obtaining infrared spectra.

One of the general advantages of IRAS is that it is frequently applied in different research areas such as Chemistry, Physics, and Biology. The technique is used to identify and characterize the chemical state, molecular structure, anisotropy, and conductivity of thin films on metallic and non-metallic surfaces. The applications of IRAS are vary in many different fields.

2.4.4.2. The Limitations

A significant limitation of IRAS currently is the difficulty in studying low-wavenumber vibration (<600 cm^{-1}). The infrared source and types of mirrors used in the FTIR are provided only in the mid-infrared region, and they cannot provide the low-energy domain. But this disadvantage will be solved by the development of more intense far-infrared sources.[10]

A specific limitation of FTIR, which is the main component of the method, is the single beam spectrum. The background spectrum measures the contribution of the instrument and the environment of the spectrum, which is measured at a different point in time than the spectrum of the sample. Ideally, the instrument and environmental contributions to the spectrum are eliminated by rationing the sample spectrum to the background spectrum.[10] So, if something in the environment changes while the sample and the background spectra are obtained, spectral artifacts can appear in the sample spectrum. The common examples are the water vapour and carbon dioxide peaks.[10] To avoid this, the one who works in the experiment has to be aware about the artifacts in order to indicate where they appear. Using this method, it would be easy to distinguish where the real peaks and the artifacts are.

One of the general disadvantages of IR spectroscopies is that it cannot detect atoms and monatomic ions. Because the single atom entities have no chemical bonds, which means there are no vibrational motions, there is no absorption of infrared radiation. Also, the noble gases like Argon and Helium cannot be detected because they exist as individual molecules.[10]

2.5. X-Ray Photoelectron Spectroscopy

The x-ray photoelectron spectroscopy is being included in the present work. This section gives an introduction to the technique and its history, then talks about its principle.

2.5.1. An Introduction and Historical Background

X-ray photoelectron spectroscopy is a widely used technique in surface science approaches because it can be applied to a broad range of materials. The technique is employed to measure the elemental composition, chemical state, the chemical formula and electronic state of the elements on the surface of a material.[13] The technique requires the UHV condition due to the measuring of freed electrons.[14]

The technique was developed by Kia Siegbahn and his group members at the University of Uppsala, Sweden in the 1960s, when they recorded the first high resolution XPS spectrum of cleaved sodium chloride (NaCl).[15] The discovery made the XPS an available instrument and Siegbahn was eventually awarded the Nobel Prize in 1981 based on his development of the technique, which was known by the acronym ESCA (Electron Spectroscopy for Chemical Analysis).[16]

2.5.2. The Principle of XPS

The principle behind the XPS is based on the photoelectric effect phenomena outlined by Einstein in 1905 where the concept was used to describe the ejection of electrons from a surface when photons impinge upon it.[13] The soft X-ray is irradiated onto the sample and then the energy of the detected electrons is analyzed, as illustrated in (Figure2.7). The photons impinge the solid surface with limited penetrating power, about 1-10 micrometers.[14] They interact with the atoms in the surface region, causing electrons to be emitted by the photoelectric effect. The kinetic energy

of emitted electrons can be measured via an electron analyzer, and illustrated by the following relation:

$$E_{\text{kinetic}} = hv - E_{binding} - \phi_s \quad (Eq\ 2.7)$$

Here hv is the photon energy, $E_{binding}$ is the binding energy of the atomic orbital from which the electron arises, and ϕ_s: is the spectrometer work function.[15]

From the equation above, the binding energy plays the main rule, which is regarded as the energy differences between the initial and final states after the photoelectrons have left the atom. The binding energy of the photoelectrons leads to the chemical identification of the elemental surface composition. Also, the number of photoelectrons emitted has a direct relationship to the concentration of the emitting atoms on the elemental surface.[15] Therefore, the spectrum is obtained as a plot of the number of detected electrons per energy interval versus their binding energy. The shift of binding energy corresponds to the change in the chemical environment.

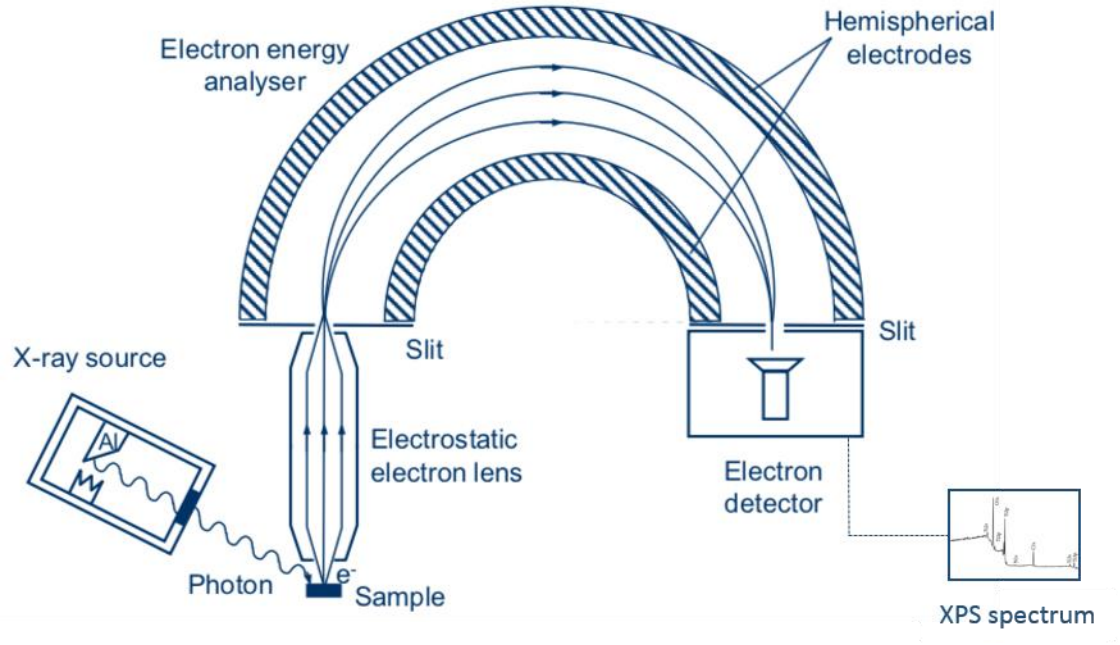

***Figure 2.7**: A schematic illustration of the X-ray photoelectron spectroscopy.*

2.6. Temperature Programmed Desorption

This section presents Temperature Programmed Desorption method included in the thesis. It includes an introduction of the TPD and the principle of the technique, both practically and theoretically.

2.6.1. Introduction of TPD

Temperature programmed desorption is a very powerful surface science method for studying molecule desorption from a solid surface by programmed heating.[17] The TPD has been specially developed in the field of catalysis because it gives a better understanding of the mechanisms of catalytic reactions, including desorption, surface reaction and adsorption.[18] The technique is applied to a system under UHV conditions.

2.6.2. The practical and theoretical Principles

The general concept behind the TPD experiments is to increase the temperature of the sample with a linear ramp and measure the rate of desorption from the surface as a function of time.[19] The adsorbents will desorb at different temperatures, depending on the desorption energy. The sample's surface is heated by raising the temperature at a programmed rate, while the amount of desorbing molecules is monitored by a quadruple mass spectrometer (QMS).[17] The increasing of temperature causes the rate of desorption, which corresponds to the amount of species left from the surface, and eventually falls to zero.[19] The sample is placed very close to the QMS in order to detect only the molecules desorbing from the front face of the surface, as shown in (Figure 2.8).[14]

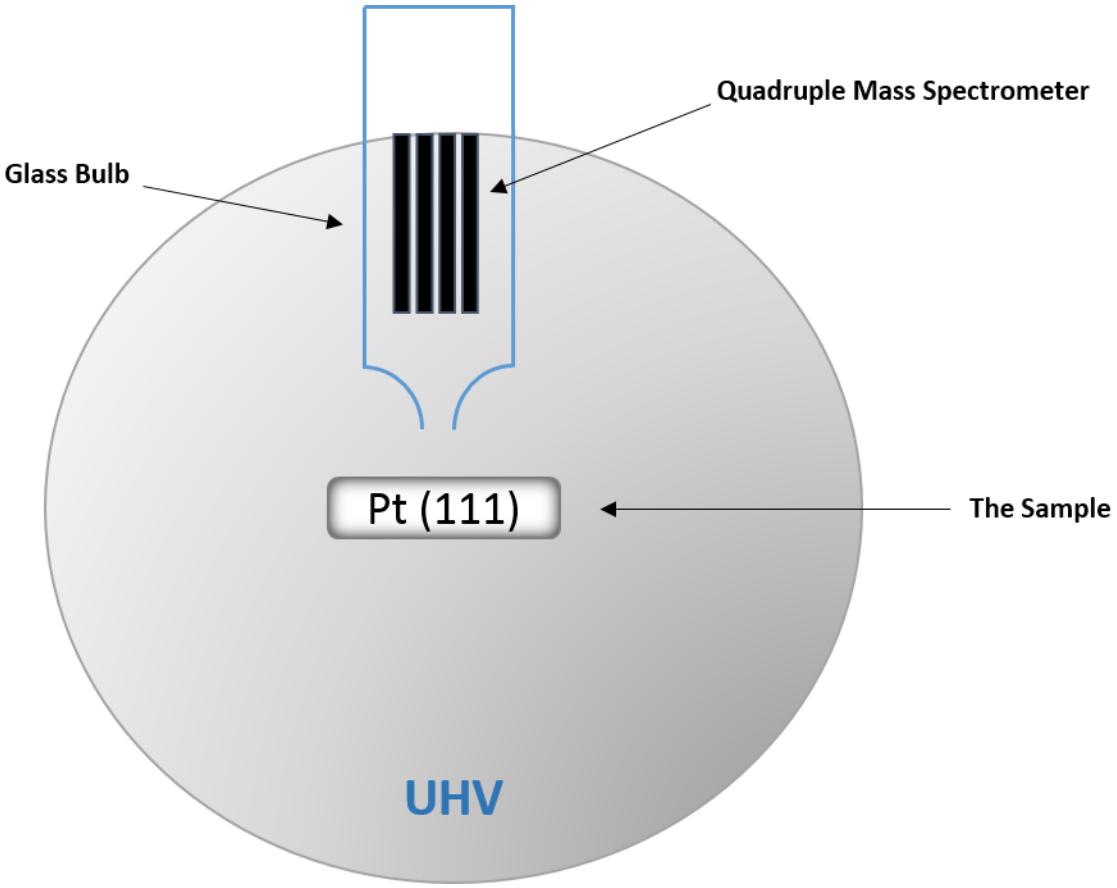

Figure 2.8: *A side diagram of the TPD technique. Adapted from reference.*[20]

The spectrum acquired from the QMS plots the mass spectrometer signal (usually measured as current and proportional to the rate of desorption) versus time (which depends on temperature according to a predetermined heating ramp).[18] In these experiments, the temperature of the sample (T) is linearly increased as a function of time (t) and can be described by the following equation:

$$T = T_0 + \beta t \qquad \therefore \beta = \frac{\partial T}{\partial t} \qquad (Eq\ 2.8)$$

Where β is the heating rate and T_0 is the initial temperature of the sample.[15]

The desorption rate is the rate of change in the coverage (θ) as a function of time and can be determined the following equation:

$$r_{des} = -\frac{\partial\theta}{\partial t} = k_{des}\,\theta^{n} \qquad (Eq\ 2.9)$$

Where k_{des} is the rate constant of desorption and n is the order of desorption.[14]

Dividing equation (2.9) by (2.8) the rate of change in the coverage as a function of temperature can be obtained:

$$-\frac{\partial\theta}{\partial T} = \frac{k_{des}\theta^{n}}{\beta} \qquad (Eq\ 2.10)$$

Assuming that the activation energy is independent of coverage, the rate constant (k_{des}) follows the Arrhenius equation:

$$k_{des} = A\exp\left(-\frac{E_{des}}{RT}\right) \qquad (Eq\ 2.11)$$

Where E_{des} is the desorption energy and R is the gas constant. The determination of the desorption energy is the main purpose of these experiments as it can be equated to the energy of adsorption of different species on the surface (adsorbate-surface binding) or to an effective activation energy for a reaction limited process (Chapter 3).

Now, from the equation (2.10) and equation (2.11) we get the following relation which is known as the Polanyi-Wigner equation:

$$-\frac{\partial\theta}{\partial T} = \frac{A\theta^{n}}{\beta}\exp\left(-\frac{E_{des}}{RT}\right) \qquad (Eq\ 2.12)$$

Equation (2.12) has two variable terms; the surface coverage (θ) and the exponential term$\left(-\frac{E_{des}}{RT}\right)$.[15] At the starting of the experiment, the exponential term is small and increases with raising the temperature, which results in an increase in the rate of desorption. The maximum

desorption rate occurs at the maximum temperature (T_{max}).[20] In contrast, at a low temperature, the surface coverage remains constant and decreases rapidly as the desorption temperature proceeds, it reaches a zero value at some temperature that gives the overall peak-like shape of the TPD profile.[15]

References:

(1) Kurt Kolasinski, D. W. *Surface Science: Foundations of Catalysis and Nanoscience Second Edition*, 2nd ed.; John Wiley & Sons, Ltd, **2008**.

(2) J.M. Walls and R. Smith. *Surface Science Techniques*, First.; Pergamon, **1994**.

(3) G. Ertl & J. Küppers. *Low Energy Electrons and Surface Chemistry*; VCH, **1985**.

(4) Park, R. M.; Hoersch, H. M. *Manual on the Use of Thermocouples in Temperature Measurement*; ASTM International, **1981**.

(5) Sigmund, P. Mechanisms and Theory of Physical Sputtering by Particle Impact. *Nucl. Instruments Methods Phys. Res. Sect. B Beam Interact. with Mater. Atoms* **1987**, *B27*,1-20.

(6) Callister, W. D. Rethwisch, D. G. *Fundamentals of Materials Science and Engineering: An Integrated Approach*; John Wiley & Sons, Ltd, 2012.

(7) Hollins, P. Infrared Reflection–Absorption Spectroscopy. *Encycl. Anal. Chem.* **2006**, *12*, 1–17.

(8) Borasio, M. Polarization Modulation Infrared Reflection Absorption Spectroscopy on Pd Model Catalysts at Elevated Pressure, Biologie, Chemie, Pharmazie, **2006**.

(9) Henning Bubert. *Surface and Thin Film Analysis: A Compendium of Principles, Instrumentation, and Applications, 2nd, Completely Revised and Enlarged Edition*; Gernot Friedbacher, H. B., Ed.; **2011**.

(10) Brain C. Smith. *Fourier Transform Infrared Spectroscopy*; CRC Press, **1996**.

(11) M.A.Chesters. Infrared Spectroscopy of Molecules on Metal Single-Crystal Surfaces. *J. Electron Spectros. Relat. Phenomena* **1986**, *38*, 123–140.

(12) T.J. Johnson; G. Zachmann. *Introduction to Step-Scan FTIR*; Bruker.

(13) JolmF. Moulder WilliamF. Stickle Peter E.'Sobol KennetlfD. Bomben. *Handbook Of X-Ray Photoelectron Spectroscopy*; Jill, C., Ed.; Perkin-Elmer Corporation, **1992**.

(14) Sims, J. J. Formic Acid Decomposition on Cobalt Surfaces, University of Ottawa, **2015**.

(15) Nadeem, M. A. Reactions of Ethanol on Bare and Noble Metal Modified TiO 2 Single Crystal and Powders, The University of Auckland, **2012**.

(16) M.Hercules, D. Electron Spectroscopy for Chemical Analysis. *J. Electron Spectros. Relat. Phenomena* **1974**, 811–826.

(17) Nava Rieman, S. Temperature Programmed Desorption Study of Dodecanethiol, Texas State University-San Marcos, **2009**.

(18) Ishii, T.; Kyotani, T. Temperature Programmed Desorption. In *Materials Science and Engineering of Carbon*. **2016**, 287–302.

(19) Joshua Erold Robert Abelard. Temperature Programmed Desorption and Infrared Spectroscopic Studies of Interfacial Hydrogen Bonds for Small Molecules Adsorbed on Silica and Within Metal Organic Frameworks, Virginia Polytechnic Institute and State University, **2017**.

(20) Cherif A. Ould Hamou. Decomposition Mechanism of Lignin Models on Pt(111) : Combining Single Crystal Experiments and First Principle Calculations, University of Ottawa, **2019**.

Chapter 3: Adsorption and Decomposition of a Lignin β-O-4 Linkage Model: Reactivity of Veratrol on Pt(111) by Combination of XPS, TPD and IRAS Experiments.

I included this collaboration work in my thesis because I performed the IRAS experiments and analysed its data. Cherif A. Ould Hamou included the first draft of the paper in his thesis. He did the analysis for TPD and XPS, and he acknowledged in his thesis that this paper will be updated and be part of my MSc's thesis. Kusuma Virginna Adiningtyas assisted in performing the XPS and TPD experiments as part of fulfillment of her coop term. Now, we obtained new data that has not been presented before. This paper will be published shortly.

Draft Manuscript in preparation for submission to Surface Science.

Adsorption and Decomposition of a Lignin β-O-4 Linkage Model: Reactivity of Veratrol on Pt(111) by Combination of XPS, TPD and IRAS Experiments

Cherif A. Ould Hamou,[†,§] Mohammed Z. Asiri,[†,§] Kusuma V. Adiningtyas, [†,‖] Javier B. Giorgi.[†,‖,*]

[†] Centre for Catalysis Research and Innovation, [§] Department of Physics, [‖] Department of Chemistry and Biomolecular Sciences, University of Ottawa, 10 Marie Curie Pvt., Ottawa, Ontario, Canada. K1N 6N5.

Abstract

To sustain the current attempts in valorizing lignin-based derivatives, the adsorption and decomposition of veratrol on a Pt(111) surface is studied as a model to understand the reactivity of the β-O-4 linkage in lignin. The results showed that under ultra-high vacuum conditions, hydrogen and carbon monoxide are the main desorbing products. Combining X-ray photoelectron spectroscopy, reflection absorption infrared spectroscopy and temperature programmed desorption experiments, a reaction mechanism is suggested, starting with the desorption of the multilayer around 215 K, followed by the decomposition of the monolayer through C-H and O-C bond cleavage on the methoxy groups. 1,2-benzoquinone is proposed to exist as a key surface intermediate that keeps decomposing to form catechol, seen for the first time in this work. Hydrogen, and carbon monoxide that are produced upon further decomposition desorb at 315 K and 420 K respectively. The appearance of a new peak at 950 cm^{-1} in the IRAS spectra is an indication of further decomposition of 1,2-benzoquinone on the Platinum surface.

Key-words: Veratrol, mechanism, decomposition, IRAS, TPD, DFT, XPS, lignin

3.1 Introduction

Lignin is one of the most abundant polymer in wood and consists of network of aromatics that are linked with each other by oxygenate groups.[1] Lignin is a sustainable and renewable feedstock that could provide an abundant supply of valuable chemicals. Among the potential routes for production of chemicals, heterogeneous catalysis is regarded as the key for lignin conversion by reducing the activation energies for reaction and targeting products selectively. In the lignin valorization quest, it becomes important to always increase the complexity of the lignin model used to have a better overall understanding of the reactivity of lignin itself. In previous published work, we started with a simple lignin model such as anisole and gradually increased the complexity of the arm moiety towards 2-phenoxyethanol.[2,3] The aromatic molecules within lignin are cross-linked with each other by more than one arm moiety and this opens new sight for investigation. Veratrol, with its two methoxy functional groups on the 1,2 positions, is used here as a model of the substituted β-O-4 linkage type (Figure 3.1).

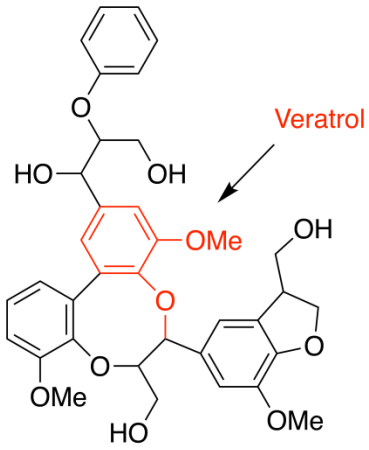

Figure 3.1: *Small lignin fragment with highlighted veratrol molecule in red. Figure adapted from reference.*[4]

No experimental or theoretical studies on the reactivity of veratrol on single crystal catalysts had yet been published. In terms of reactivity, veratrol can undergo a decomposition scheme that is, in principle, related to aromatics containing similar functional groups, such as anisole and guaiacol (2-Methoxyphenol). As such, previous studies of the reactivity of anisole and guaiacol on Pt(111) are relevant.

The reactivity of anisole on Pt(111) has been studied by means of temperature programmed desorption, X-ray photoelectron spectroscopy and reflection absorption infrared spectroscopy. In summary, anisole desorbs from the Pt(111) surface in two stages, the multilayer at 260 K and small fraction of the monolayer at 360 K.[2] The core level binding energies of C 1s showed two major peaks at 283.7 and 285.3 eV that were attributed to carbon species bound to a carbon atom and carbon species bound to an oxygen atom respectively. Most of the monolayer decomposes into phenoxy via a C-H bond cleavage on the methyl group below 325 K. At higher temperatures, there is a competition between Ph-O bond cleavage, forming phenyl then benzene, and a complete decomposition of the aromatic ring. These results showed that under UHV conditions, the formation of benzene is dominant and it desorbs from the surface at 400 K. Above 450 K, the remaining phenoxy completely decomposes into CO and H_2.[2,5,6]

The reactivity of Guaiacol has been studied on Pt(111) by means of surface science technique and first principle calculations. The decomposition of the guaiacol starts with the dehydrogenation of the arm moieties. Vohs and coworkers[7] studied the reactivity of guaiacol on Pt(111) by means of temperature programmed desorption and high energy electron loss spectroscopy. On Pt(111), the physisorbed layer of guaiacol desorbs from the surface at 225 K. The chemisorbed layer simply decomposes by dehydrogenation of the hydroxyl group to form 2-methoxy-2,5-cyclohexadien-1-one as key intermediate. Further heating to 285 K, the intermediate

starts to decompose and the observed desorption byproducts are CO that desorbs at 435 K and H_2 that desorbs at 340 K and 435 K. Upon reaching 485 K, only hydrocarbons remain on the surface.

McEwen and coworkers[8], on the other hand, studied the reactivity of guaiacol on Pt(111) by means of a temperature programmed X-ray photoelectron spectroscopy and first principles calculations. Guaiacol was adsorbed on the surface at 170 K and two major signals in the C 1s region corresponding to hydrocarbons/aromatic carbon species and carbon bound to oxygen species are found at 284.4 and 286.2 eV respectively. The desorption of the physisorbed layer was observed at 240 K. Although the overall binding energies remain unchanged, the use of synchrotron based XPS allowed to distinguish the different carbon species and it was reported that the saturation of the monolayer does not occur without some decomposition of guaiacol. At 170 K, the physisorbed and chemisorbed layers, in addition to some decomposed guaiacol are simultaneously present on the surface. Upon heating to 375 K, guaiacol decomposes by either the dehydrogenation of the hydroxyl group or the methyl group to eventually form 1,2-benzoquinone as key intermediate. Above 375 K, the 1,2-benzoquinone keeps decomposing to form carbonaceous species and CO that quickly desorb from the surface.

Vlachos and coworkers[9], studied the reaction mechanism of guaiacol hydrogenation on Pt(111) by means of density functional theory calculations and linear free energy relations. guaiacol adsorbs flat on the surface via all the carbon atoms in the aromatic ring. The decomposition of guaiacol starts with the dehydrogenation of the methyl group. The intermediate specie can undergo two distinct reaction pathways to form a quinone radical specie as a key intermediate specie that will eventually get hydrogenated to form catechol. The first reaction pathway involves further dehydrogenation of the methyl group or demethylation. The second

pathway will undergo O-H bond cleavage followed by dehydrogenation of the methyl group. The formation of phenol is speculated on further decomposition of the catechol on the surface.

Heyden and coworkers[10], studied the reaction mechanism of guaiacol hydrogenation on Pt(111) by means of density functional theory calculations and microkinetic modeling. Guaiacol decomposes into two different reaction pathways that involve either the dehydration of the methyl group or the hydroxyl group to eventually form 2-hydroxyphenolate as a key intermediate. Then the intermediate specie gets hydrogenated to form catechol as the major byproduct. The formation of anisole and phenol is proposed as well but the deoxygenation of the intermediate specie is 4 orders magnitude slower than production of catechol.

Building on previous experiments with anisole and 2-phenoxyethanol, but considering the uncertainty in reaction pathways and intermediates observed for guaiacol, similar but more complex molecules require detailed study. This work provides a detailed description of the interaction and decomposition of veratrol on a Pt(111) surface. The focus is on the influence of the second arm moiety with regard to the reaction selectivity. The study is conducted by means of X-ray photoelectron spectroscopy (XPS), infrared reflection absorption spectroscopy (IRAS) and temperature programmed desorption (TPD).

3.2 Experimental

XPS and TPD experiments were performed under ultrahigh vacuum (UHV) in a stainless steel analysis chamber with a base pressure of 5×10^{-10} mbar. The Pt(111) crystal surface was cleaned by repetitive cycles of 15 min of sputtering (0.5 keV, 1×10^{-5} mbar Ar^+) at 600 K, followed by annealing to 1100 K, described in detail previously.[2]

IRAS experiments were carried out in another UHV chamber dedicated for reflection absorption infrared spectroscopy where the base pressure is 7 x 10^{-10} mbar. The Pt (111) crystal surface was cleaned by repetitive cycles of 30 mins of sputtering (1.5 keV, 1 x 10^{-5} mbar Ar^{+}) at 600 K, followed by annealing to 1100 K for 2 mins. The sample cleanliness was confirmed by LEED. Detailed description of the chamber can be found in chapter 5.

Veratrol (+99% purity, Sigma Aldrich) was introduced to the UHV chamber through a leak valve that was connected to a gas manifold with an attached veratrol reservoir. The reservoir was heated to 473 K to increase the vapor pressure and ensure the purity of the deposition. The gas manifold was heated accordingly to prevent condensation and allow a constant, stable flux of veratrol gas into the chamber. Exposure of veratrol to the surface was typically performed at 1x10^{-7} mbar pressure and the dosage measured in Langmuirs (1 L = 1.33x10^{-6} mbar ● s).

3.2.1 XPS

XPS spectra were recorded on a Specs GmbH system (XR50 X-ray source and Phoibos 100 SCD analyzer) using a standard Al Kα source (1486.7 eV) operated at 380 W (14.6 kV, 26 mA). Selected peaks were obtained in high resolution spectra using 0.1 eV step size, 0.5 second dwell time, and pass energy of 30 eV. For the C 1s and O 1s regions 6 scans were acquired to increase the signal to noise ratio. The spectra were then fit using CasaXPS analysis software using a mixed Gaussian-Lorentzian function and Shirley background subtractions for the C 1s region while a Linear background subtraction was used for the O 1s region.

For the experiments, veratrol was dosed on the clean sample at 130 K and then heated up to the desired temperature of observation to acquire the spectrum. Once the acquisition was done, the sample was subject to a cleaning cycle (Ar^{+} sputtering followed by annealing to 1100 K) to

remove all the residual carbon on the surface. The cleanliness of the sample surface was verified by LEED and XPS.

3.2.2 TPD

The TPD experiments require the placing of the sample in front of a differentially pumped quadrupole mass spectrometer (QMS) and ramping up the sample temperature while monitoring the fragments of interest. For our experiments, the Pt(111) sample was dosed with varying exposures of veratrol at 110 K and placed 1 mm below a 1 mm diameter hole leading to the differentially pumped QMS. The temperature-controlled heating ramp was programmed in LabVIEW and designed to provide and record a linear temperature ramp in the range of 120 K to 800 K, with a ramp rate of 6 K/s. The sample was subject to one cleaning cycle (Ar^+ sputtering followed by annealing to 1100 K) to ensure the cleanliness of the surface before each dosage. A total of 11 channels corresponding to m/z values of 138, 110, 108, 94, 78, 32, 31, 28, 16, 14 and 2, were monitored for the veratrol TPD experiments. The selected m/z values correspond to the expected species and their respective fragmentation patterns.

Analysis of the TPD data allows the experimental determination of desorption energies E_{des} for veratrol. The analysis is performed based on the general rate law for desorption by the simple approach of Redhead[11] with appropriately corrected frequency factors. The calculated frequency factors **ν** are presented in Table 3.2 as obtained using the Campbell approach[12,13] for molecular desorption and temperature corrected entropy values from the Knovel's Database.[14] The entropy of veratrol is not available; the entropy value for guaiacol was used as an approximation.

3.2.3 IRAS

The IRAS experimental spectra were collected at 4 cm^{-1} resolution with 1000 scans. The molecules were dosed on the clean sample at 130 K and then heated up to the desired temperature of observation to acquire the spectrum. For temperatures above 400 K, the sample was heated to the desired temperature and then cooled down to 400 K to acquire the spectrum. The spectra were manipulated using OPUS analysis software by performing a baseline correction and an atmospheric compensation for the CO_2 and H_2O regions. Due to geometry and different setup, the dosage in the IRAS chamber is different from the analysis chamber of the TPD and XPS. Dosage values are reported and the discussion is performed in terms of comparable relative coverage.

3.3 Results

3.3.1 XPS

Preliminary XP spectra was initially presented by Ould Hamou.[4] Subsequently, data was collected and analyzed multiple times to improve data quality and confirm initial interpretations. The identification of surface species upon dosing veratrol on Pt(111) was initially performed by monitoring the carbon and oxygen environment of species on the surface as a function of temperature. Figure 3.2. shows C 1s and O 1s photoelectron spectra after deposition of 20 L of veratrol on Pt(111) at 130 K, with spectra acquired at varying temperatures. Upon deposition, at 130 K, veratrol shows two peaks in the C 1s spectra, one at 285.4 eV, which is attributed to carbon atoms bound to an oxygen atom (labeled C-O), and the other one at 283.6 eV which is attributed to carbon atoms bound only to other carbon or hydrogen atoms (labeled C-C). The binding energy difference between the carbon peaks is 1.8 eV. After flashing to 180 K, the peak areas and binding energies remain constant. At 240 K, the C-C and C-O peak areas decrease in intensity as some desorption takes place and the binding energy difference of the C 1s signals of the C-C and C-O

peaks remain the same. At 300 K, the C-C and C-O areas decrease in intensity and shift to lower binding energies of 283.3 and 284.9 eV respectively. The difference in binding energy is 1.6 eV. At 360 K, the C-C and C-O areas decrease in intensity and shift to lower binding energies of 283.1 and 284.7 eV respectively. Upon heating to 450 K, the C-O peak area vanishes and C 1s area peak decreases as only adventitious carbon remains on the surface.

Observations of the O 1s region after depositing 20 L of veratrol at 130 K on Pt(111) correlates with observations in the C 1s region. Upon deposition, at 130 K, veratrol shows one peak at 532.3 eV. After flashing to 180 K, the peak area and binding energy remain constant. At 240 K, the peak area intensity decreases and shifts to lower binding energy of 531.8 eV as some desorption and decomposition takes place. At 300 K, the peak area intensity decreases and shifts to lower binding energy of 531.7 eV as some desorption and decomposition takes place. This is consistent with the observations made on the C 1s region. At 360 K, the peak area intensity decreases and shifts to a lower binding energy of 531.6 eV, as some desorption and decomposition occur from the surface. At 450 K, the peak area vanishes.

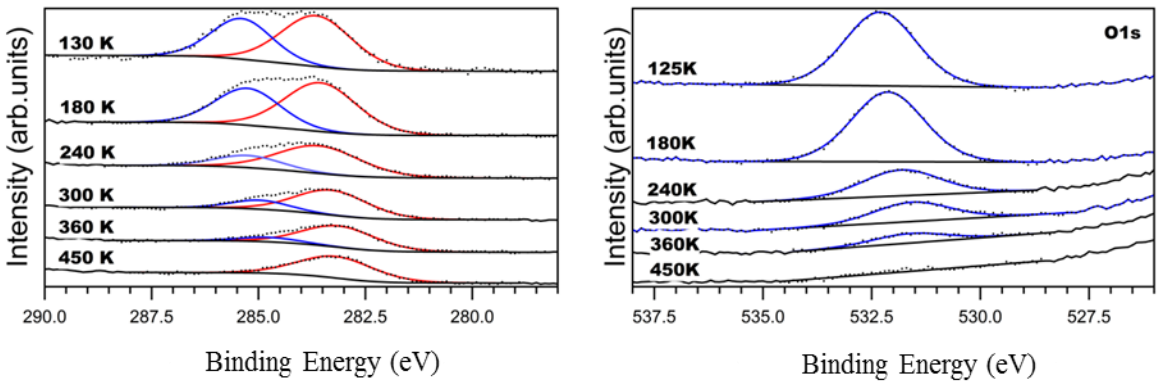

***Figure 3.2**: XPS spectra acquired at different temperatures for 20 L of veratrol deposited at 130 K.*

Integrating the area of the C 1s region gives insight on how the coverage changes as a function of temperature (Figure 3.3). The drop in C 1s peak area above 200 K corresponds to desorption of the multilayer as will be further discussed in comparison with TPD results.

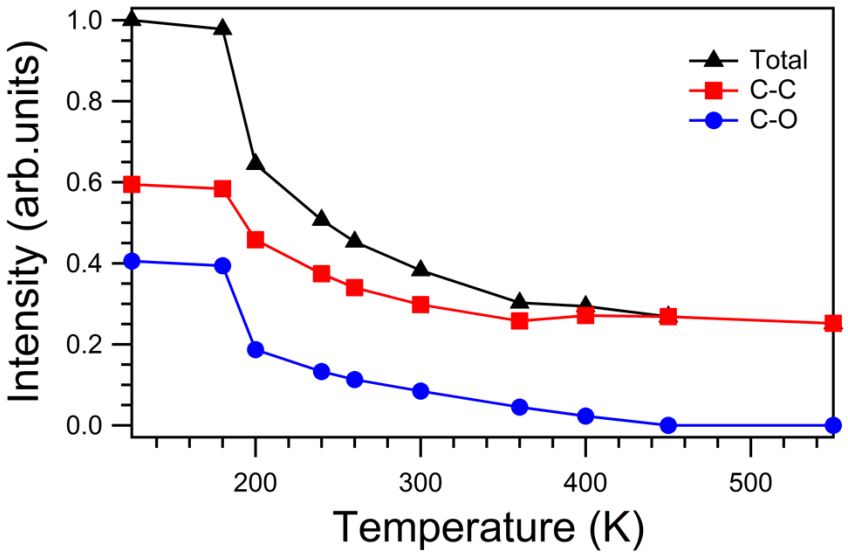

Figure 3.3: *Analysis of XPS spectra acquired at different temperatures for 20 L of veratrol deposited at 130 K. The peak area decreases after 180 K, which corresponds to desorption of the multilayer.*

3.3.2 IRAS

The geometry and setup of the IRAS chamber is different from the analysis one, hence the dosage between the two chambers cannot be directly compared.

Figure 3.4 shows the vibrational spectra of veratrol after deposition of 200 L of veratrol at 130 K, with spectra acquired at varying temperatures. Upon deposition, at 130 K, veratrol shows seven major peaks in the spectra at 758, 1033, 1127, 1261, 1467, 1515 and 1595 cm^{-1}. The peaks at 1515 and 1595 cm^{-1} are assigned to C-C ring + CCO stretches and the peak at 758 cm^{-1} to C-H

bending out of plane. The more relevant peaks assigned to O-CH_3 stretching are observed at 1033 and 1055 cm^{-1} whereas the Ph-O + C-C stretches are assigned at 1233 and 1261 cm^{-1}. Weak peaks corresponding to CH_3 stretching modes are observed at 2836, 2958, 3004 cm^{-1} whereas CH_3 scissor modes are observed at 1443 and 1467 cm^{-1}. Finally, a very weak C-H stretching peak is also observed at 3064 cm^{-1}.

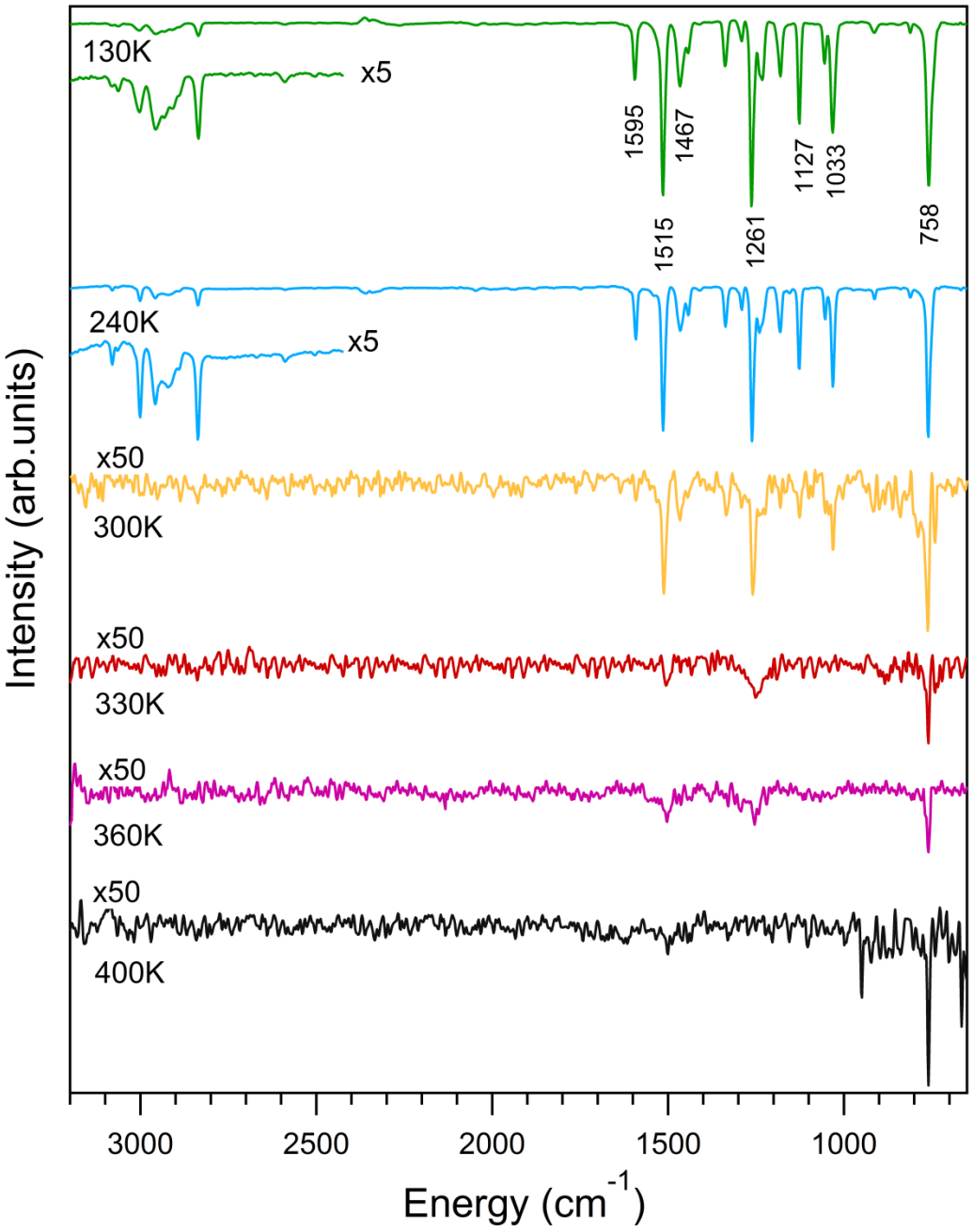

Figure 3.4: *IRAS spectra acquired at different temperatures for 200 L of Veratrol deposited at 130 K. Spectra have been offset for clarity. Although initially presented as part of Ould Hamou's thesis* [4]*, since it was written in paper format, this data is my work.*

The identification of surface species upon dosing multilayers of veratrol on Pt(111) was performed by monitoring vibrational modes of species on the surface as a function of temperature. Details of the band assignments and comparison to the vibrational frequencies of liquid anisole are presented in Table 3.1.

Table 3.1: *Vibrational modes and peak assignments of veratrol on Pt(111).*

Vibrational mode [a]	**Pt(111)**	**Gas Phase (exp)**[15]	**Calculated**[15]
(a) arm vibrations			
CH3 asym. ip. str.	**3004**	**3000**	**3039**
CH3 asym. op. str.	**2958**	**2954**	**2971**
CH3 sym. op. str.	**2836**	**2835**	**2898**
HCH (CH_3) scissor	**1467**	**1463**	**1457**
HCH (CH_3) scissor	**1443**	**1442**	**1435**
CH_3 scissor	**1335**	**1330**	**1421**
CH_3 rock	**1181**	**1176**	**1157**
O-CH_3 str.	**1055**	**1052**	**1042**
O-CH_3 str.	**1033**	**1028**	**1019**
(b) ring vibrations			
C-H str.	**3064**	**3064**	**3065**
C-C ring + CCO str.	**1595**	**1592**	**1563**
C-C ring + CCO str.	**1515**	**1506**	**1480**
Ph-O sym. + C-C str. + CH bend	**1261**	**1254**	**1255**
Ph-O asym. + C-C str. + C-H bend	**1233**	**1230**	**1211**
C-H bend	**1127**	**1123**	**1096**
C-H bend	**915**	**------**	**------**
Ring breathing	**810**	**------**	**------**
C-H bend (out of plane)	**758**	**------**	**------**

[a]Approximate mode description; str, stretching; sym/asym, symmetric/asymmetric; ip, in plane; op, out of phase.

There are small shifts between the vibrational modes of gas phase veratrol and the ones observed on Pt(111) mainly due to surface/metal interaction. As above, due to metal surface selection rules, only the modes that have vibrational dipole moments perpendicular to the surface can be observed and this gives us an insight about the adsorption geometry of the molecule on the surface. The observation of strong C-H bending peaks at 758, 915, and 1127 cm^{-1} indicates that veratrol adsorbs on the surface primarily via carbon atoms of the aromatic ring. Furthermore, the observation of O-CH_3, Ph-O + C-C, C-C ring + CCO stretches and C-H stretching peaks indicates that the methoxy groups of the veratrol are tilted away from the surface. These observations are in agreement with previous suggestions for anisole and guaiacol adsorption on Pt(111).[2,5,9,10,16] After increasing the temperature to 240 K, the majority of the IR peak intensities remain the same except for the peaks at 2958, 3004 and 3064 cm^{-1}. These peaks become stronger and sharper. This behavior is attributed to the rearrangement of molecules in the adsorbed layer to a more thermodynamically stable geometry.

Upon reaching 300 K, the IR peaks decrease in intensity which is in agreement with the temperature range of the molecular desorption of the multilayer observed in the XPS. The peaks corresponding to C-H stretching modes in the CH_3 fragment, observed at 2836, 2958, 3004 cm^{-1}, vanish and the constant presence of the 1033 and 1261 cm^{-1} assigned to O-CH_3 stretching and Ph-O + C-C stretching suggest that the veratrol started decomposing by C-H bond cleavage on the methyl group. Further heating to 330 K leads to the disappearance of the peaks at 1033, 1335 and 1467 cm^{-1} corresponding to O-CH_3 stretching, CH_3 rocking and HCH scissoring respectively. These observations clearly indicate the cleavage of the methyl group, inferring the formation of 1,2-benzoquinone species on the surface. Furthermore, the peaks at 758, 1261 and 1515 cm^{-1} shift

and the disappearance of the C-H bending mode at 1127 cm^{-1} are associated with the loss of aromaticity in the ring which emphasizes the formation of 1,2-benzoquinone species.

The intermediate specie seems to be stable up to 360 K. At 400 K, the peak at 1261 cm^{-1} vanish while a new peak emerges at 950 cm^{-1} and the peak at 758 cm^{-1} gets stronger which suggests that the ring breaks down as the molecule completely decomposes. In addition, no molecular CO stretching peak has been observed in the 1800-2100 cm^{-1} region, which suggests that the reported desorption of CO from veratrol decomposition is reaction-limited.

3.3.3 TPD

Preliminary TPD data was presented by Ould Hamou in his thesis.[4] Since then, TPDs were collected multiple times. While the desorption energy of veratrol and its hydrogen and carbon monoxide products were corroborated, the observation of new species was used to interpret the mechanism in new light. This data has greatly improved the importance of the manuscript and it is an important part of my work.

Molecular desorption of the parent veratrol molecule was monitored at a high coverage as a function of temperature (Figure 3.5). The data shows that, at early temperatures, the molecular desorption peak of veratrol occurs at 215 K. This peak is attributed to the desorption of the multilayer. Previous studies of closely related aromatics have reported similar temperatures and behavior for the physisorbed layer.[2,3,7,8,17] The only other observed reaction products of the decomposition of veratrol are catechol, H_2 and CO. The TPD spectrum for the catechol fragments (Figure 3.5b) shows that for 3.2 L coverage, catechol molecularly desorbs from the surface with a peak at 360 K. As the coverage increases, the peak intensity remains unchanged. The dosage dependence, particularly the lack of observed desorbing aromatics at lower coverages, is in

agreement with previous literature where it was also shown that aromatics such as benzene, phenol, anisole and 2-phenoxyethanol decompose completely on the Pt(111) surface for coverages below 0.6 ML.

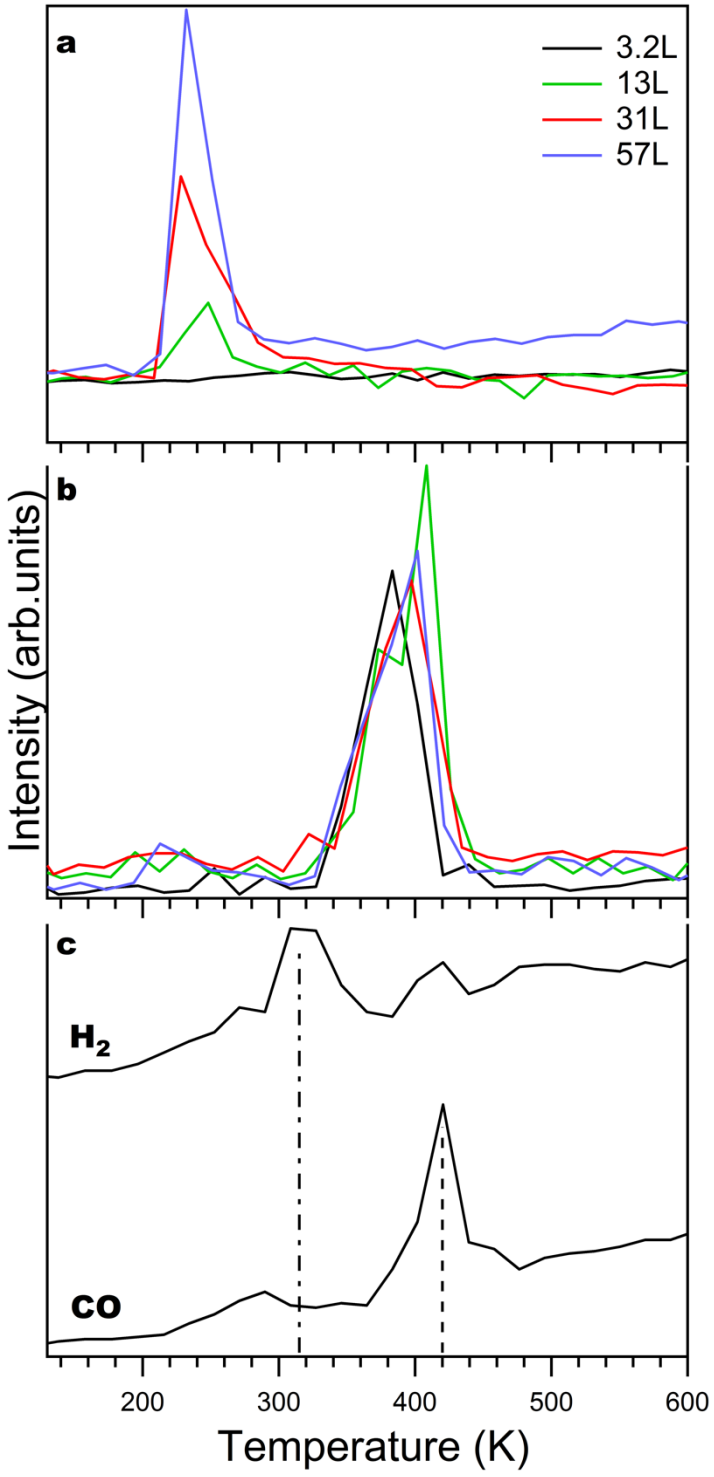

Figure 3.5: *TPD spectra after veratrol exposure on Pt(111) and selecting veratrol and formed byproducts (Catechol, Hydrogen and Carbon-monoxide). Different exposures of veratrol have been dosed at 130 K on Pt(111) and desorption rates are measured using a linear temperature ramp of 6 K/s. The line*

for dashed CO corresponds to molecular desorption of pure CO from Pt(111) with 0.33 ML coverage.[18,19]*The dot-dashed line for H_2 corresponds to desorption temperature of Hydrogen with 2 L coverage from Pt(111).*[20,21]

Hydrogen shows peaks at 315 K, 420 K and 470 K. In comparison, the associative desorption of hydrogen from Pt(111) has been previously observed in the temperature interval between 290-375 K.[20,21] This suggests that the desorption peak at 315 K is more likely to be desorption-limited and the peaks at 420 K and 470 K are reaction-limited. In contrast, CO desorbs with one peak at 420 K and this corresponds to the molecular desorption of pure CO from Pt(111) with a 0.33 ML coverage.[18,22] The coincidence of the desorption temperature and the sharpness of the CO peak and the second hydrogen peak suggest that the desorption of CO is also reaction-limited and that they are the byproduct of a common intermediate species. At this point it is more likely that the aromatic ring is starting to decompose on the surface. Similar behavior has been observed with oxygenated aromatic molecules (anisole, 2-phenoxyethanol and phenol) adsorbed on Pt(111).[2,3,5,17] No other molecular products have been observed.

Table 3.2: *Desorption energies of observed species, calculated by Redhead analysis of the TPD data.*

Species	**Observations**	**Temperature (K)**	**ν^a (s^{-1})**	**E_{des} (kJ/mol)**
Veratrol	Multilayer	215	3.34×10^{15}	64.8
Catechol	Molecular desorption	360	9.24×10^{16}	118
Carbon monoxide	Molecular desorption	420	3.95×10^{14}	119
	Literature	410[23]	-------	-------
Hydrogen	Analyzed as molecular desorption	315	2.62×10^{13}	82.2
		420	3.73×10^{13}	111
		470	4.28×10^{13}	126

3.4 Discussion

From IRAS, XPS and TPD experimental results, a schematic of the reaction and decomposition of veratrol on Pt(111) is proposed in (Figure 3.6). Upon dosing, veratrol adsorbs on the Pt(111) surface at 130 K. Upon heating, the physisorbed layer molecularly desorbs at 215 K. The desorption energy of the multilayer is 64.8 kJ/mol and it is agreement with the enthalpy of vaporization of 68.1 kJ/mol of veratrol.[24]

The first saturated layer totally decomposes on the surface as the temperature is increased and the only observed byproducts are catechol, CO and H_2. At 300 K, the C 1s binding energy difference between the C-C and C-O XPS peaks reduces to 1.6 eV, suggesting the onset of decomposition of the parent molecule. The associative desorption of H_2 at 315 K (which corresponds to "usual' temperature desorption of H_2) is another clear indication of the decomposition of the parent molecule. Furthermore, the peaks corresponding to CH_3 stretching modes observed at 2836, 2958, 3004 cm^{-1} at 300 K, clearly indicate that the dehydrogenation occurred on the methyl group. This is in agreement with previously published studies of phenol, anisole, 2-phenoxyethanol and guaiacol on Pt(111) showing that the first reaction step starts with the dehydrogenation of the arm below 300 K.[2,3,5,7–10,17] Upon heating to 330 K, we observe further changes in the IR spectrum, the disappearance of the peaks at 1033 and 1127 cm^{-1} corresponding to O-CH_3 stretching and C-H bending mode respectively and the presence of the peaks at 760 and 1250 cm^{-1} corresponding to C-H bending out of the plane and Ph-O+C-C stretching respectively suggest that the molecule lost its aromaticity. The IR spectrum of 1,2-benzoquinone has vibrational peaks at 739, 1262 and 1734 cm^{-1} which are attributed to C-H wag, C-C stretch + C-H bend and C–C=O stretch respectively. Heyden and coworkers[10] studied guaiacol on Pt(111) and suggested 1,2-benzoquinone to be as an intermediate in the possible decomposition pathways of guaiacol on

Pt(111). They showed that the adsorption energy of 1,2-benzoquinone is ~281 kJ/mol and the most stable adsorption geometry to be flat with two oxygen atoms parallel to the surface. Thus, the peak at 1734 cm^{-1} cannot be observed in our study due to metal selection rules. In fact, a clear observation of the C–C=O stretch is seen in the data of Vohs et al.[7] The HREELS data for guaiacol/Pt(111) shows that the intermediate species of the decomposition loses its aromaticity at 285 K. A peak at ~1740 cm^{-1} starts to appear at 285 K and disappears between 400-480 K. This peak, which was not identified by the authors, is consistent with the formation of 1,2-benzoquinone, emphasizing that this species adsorbs in a flat geometry on the surface and keeps decomposing above 400 K. Desorption of catechol and carbon monoxide correlates with the disappearance of the C-O peak in C 1s and in the O 1s region at 360 K, and the appearance of a new peak at 950 cm^{-1} indicates further decomposition of the 1,2-benzoquinone. The calculated desorption energy of catechol is 118 kJ/mol. Only hydrocarbons and adventitious carbon remain on the surface at 450 K. This is consistent with the previous reported results of the decomposition of 1,2-benzoquinone on Pt(111) surface.

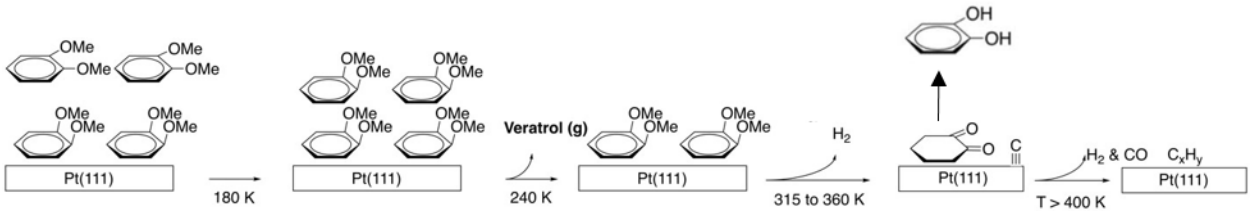

Figure 3.6: *Proposed pathway of veratrol decomposition under UHV conditions on Pt(111) built from surface science experiments. Figure adapted and updated form reference.*[4]

3.5 Conclusion

In ultra-high vacuum conditions, veratrol adsorbs on the surface at 130 K. The multilayer desorbs at 230 K and the monolayer starts decomposing by dehydrogenation of the methyl group below 300 K. The only observed decomposition by products are H_2 and CO. 1,2-Benzoquinone seems to be key intermediate in the decomposition pathway of veratrol. The emergence of a new peak at 950 cm^{-1} in the IRAS spectra is an identification of further decomposition of 1,2-Benzoquinone on Pt(111) surface. It seems that increasing the complexity by having a methoxy arm attached in the ortho position opened a new catalytic pathway towards the production of catechol. The observation of this alcohol is a significant novelty of the showed results that is not observed before in mono-substituted molecules.

References:

(1) Zakzeski, J.; Bruijnincx, P. C. A.; Jongerius, A. L.; Weckhuysen, B. M. The Catalytic Valorization of Ligning for the Production of Renewable Chemicals. *Chem. Rev.* **2010**, *110*, 3552–3599.

(2) Reócreux, R.; Ould Hamou, C. A.; Michel, C.; Giorgi, J. B.; Sautet, P. Decomposition Mechanism of Anisole on Pt(111): Combining Single-Crystal Experiments and First-Principles Calculations. *ACS Catal.* **2016**, *6*, 8166−8178.

(3) Ould Hamou, C. A.; Réocreux, R.; Sautet, P.; Michel, C.; Giorgi, J. B. Adsorption and Decomposition of a Lignin β-O-4 Linkage Model, 2-Phenoxyethanol, on Pt(111): Combination of Experiments and First-Principles Calculations. *J. Phys. Chem. C* **2017**, *121*, 9889−9900.

(4) Cherif A. Ould Hamou. Decomposition Mechanism of Lignin Models on Pt(111) : Combining Single Crystal Experiments and First Principle Calculations, University of Ottawa, **2019**.

(5) Shi, D.; Arroyo-Ramírez, L.; Vohs, J. M. The Use of Bimetallics to Control the Selectivity for the Upgrading of Lignin-Derived Oxygenates: Reaction of Anisole on Pt and PtZn Catalysts. *J. Catal.* **2016**, *340*, 219–226.

(6) Tan, Y. P.; Khatua, S.; Jenkins, S. J.; Yu, J. Q.; Spencer, J. B.; King, D. A. Catalyst-Induced Changes in a Substituted Aromatic: A Combined Approach via Experiment and Theory. *Surf. Sci.* **2005**, *589*, 173–183.

(7) Shi, D.; Vohs, J. M. TPD and HREELS Study of the Reaction of Guaiacol on Zn-Decorated Pt(111). *Catal. Today* **2018**, *302*, 272–276.

(8) Hensley, a. J. R.; Wöckel, C.; Gleichweit, C.; Gotterbarm, K.; Papp, C.; Steinrück, H.-P.; Wang, Y.; Denecke, R.; McEwen, J.-S. Identifying the Thermal Decomposition Mechanism of Guaiacol on Pt(111): An Integrated X-Ray Photoelectron Spectroscopy and Density Functional Theory Study. *J. Phys. Chem. C* **2017**, *122*, 4261− 4273

(9) Lee, K.; Gu, G. H.; Mullen, C. A.; Boateng, A. A.; Vlachos, D. G. Guaiacol Hydrodeoxygenation Mechanism on Pt(111): Insights from Density Functional Theory

and Linear Free Energy Relations. *ChemSusChem* **2015**, *8*, 315–322.

(10) Lu, J.; Behtash, S.; Mamun, O.; Heyden, A. Theoretical Investigation of the Reaction Mechanism of the Guaiacol Hydrogenation over a Pt(111) Catalyst. *ACS Catal.* **2015**, *5*, 2423–2435.

(11) Redhead, P. A. Thermal Desorption of Gases. *Vacuum* **1962**, 203–211.

(12) Campbell, C. T.; Sellers, J. R. V. Correction to "The Entropies of Adsorbed Molecules." *J. Am. Chem. Soc.* **2013**, *135*, 13998–13998.

(13) Campbell, C. T.; Sellers, J. R. V. The Entropies of Adsorbed Molecules. *J. Am. Chem. Soc.* **2012**, *134*, 18109–18115.

(14) *Knovel Critical Tables (2nd Edition)*.

(15) Lucarelli, C.; Giugni, A.; Moroso, G.; Vaccari, A. FT-IR Investigation of Methoxy Substituted Benzenes Adsorbed on Solid Acid Catalysts. *J. Phys. Chem. C* **2012**, *116*, 21308–21317.

(16) Réocreux, R.; Huynh, M.; Michel, C.; Sautet, P. Controlling the Adsorption of Aromatic Compounds on Pt(111) with Oxygenate Substituents: From DFT to Simple Molecular Descriptors. *J. Phys. Chem. Lett.* **2016**, *7*, 2074–2079.

(17) Ihm, H.; White, J. M. Stepwise Dissociation of Thermally Activated Phenol on Pt(111). *J. Phys. Chem. B* **2002**, *104*, 6202–6211.

(18) Steininger, H.; Lehwald, S.; Ibach, H. On the Adsorption of CO on Pt(111). *Surf. Sci.* **1982**, *123*, 264–282.

(19) Norton, P. R.; Davies, J. A.; Jackman, T. E. Absolute Coverages of CO and O on Pt(111); Comparison of Saturation CO Coverages on Pt(100), (110) and (111) Surfaces. *Surf. Sci.* **1982**, *122*, 593–600.

(20) Christmann, K.; Ertl, G.; Pignet, T. Adsorption of Hydrogen on a Pt(111) Surface. *Surf. Sci.* **1976**, *54*, 365–392.

(21) Lu, K. E.; Rye, R. R. Flash Desorption and Equilibration of H2 and D2 on Single Crystal Surfaces of Platinum. *Surf. Sci.* **1974**, *45*, 677–695.

(22) Norton, P. R.; Goodale, J. W.; Selkirk, E. B. Adsorption of Co on Pt(111) Studied by Photoemission, Thermal Desorption Spectroscopy and High Resolution Dynamic Measurements of Work Function. *Surf. Sci.* **1979**, *83*, 189–227.

(23) Payne, S. H.; McEwen, J. S.; Kreuzer, H. J.; Menzel, D. Adsorption and Desorption of CO on Pt(111): A Comprehensive Analysis. *Surf. Sci.* **2005**, *545*, 47–69.

(24) Matos, M. A. R.; Miranda, M. S.; Morais, V. M. F. Calorimetric and Theoretical Determination of Standard Enthalpies of Formation of Dimethoxy- and Trimethoxybenzene Isomers. *J. Phys. Chem. A* **2000**, *104*, 9260–9265.

Chapter 4: Adsorption and Decomposition of a Lignin β-O-4 Linkage Model: Reactivity of Veratrol, 1,3-dimethoxybenzene, and 1,4-dimethoxybenzene on Pt(111).

I performed all the experiments, acquired and analysed all data in this chapter. This chapter builds on the pervious chapter focussed on veratrol by comparing the positional isomers 1,2-dimethoxybenzene (veratrol), 1,3-dimethoxybenzene and 1,4-dimethoxybenzene. Insights regarding molecular geometry and reactivity are sought based on IRAS data. This manuscript (chapter 4) will be sent for publication shortly.

Draft Manuscript in preparation for submission to Surface Science.

Adsorption and Decomposition of a Lignin β-O-4 Linkage Model: Reactivity of Veratrol, 1,3-dimethoxybenzene, and 1,4-dimethoxybenzene on Pt(111).

Mohammed Z. Asiri,[†,§] Javier B. Giorgi.[†,‖,*]

[†] Centre for Catalysis Research and Innovation, [§] Department of Physics, [‖] Department of Chemistry and Biomolecular Sciences, University of Ottawa, 10 Marie Curie Pvt., Ottawa, Ontario, Canada. K1N 6N5.

Abstract

Under ultrahigh vacuum conditions, the decomposition of Veratrol, 1,3-dimethoxybenzene, and 1,4-dimethoxybenzene on Pt(111) is studied as a model to understand the reactivity of the β-O-4 linkage in lignin. Comparing IRAS data for 1,3-dimethoxybenzene and 1,4-dimethoxybenzene with Veratrol's comprehensive data leads to observation of the desorption of the multilayer and monolayer as well as the generation of decomposition products. Although the chemical composition and types of bonds are the same in the three molecules, the positional variation in the isomers leads to different adsorption geometries, desorption energies and reactivity.

Key-words: Veratrol, 1,3-dimethoxybenzene, 1,4-dimethoxybenzene, Desorption, mechanism, decomposition, IRAS, lignin.

4.1. Introduction

The demand of energy increases staidly with the increasing world population, requiring new resources of energy that are widely available and sustainable. Biomass is a promising resource to reduce the dependence on fossil fuels and its rich chemistry makes it a good source for a variety of applications. Biomass conversion can be used in chemical production since it is renewable, inexpensive, and widely available, and thus the conversion of biomass into high value products is an important target both economically and socially. In particular, lignocellulosic biomass is one of the most abundant components in plants including trees, seaweeds, crops and animal wastes.[1] Lignin is the second most abundant lignocellulosic polymer in wood which represents up to 40% of the dry biomass weight.[1,2] Due to its unique structure and chemical properties, several of fine and bulk chemicals can be obtained from lignin.[3,4] Lignin conversion has been studied by different methods such as pyrolysis, hydrothermal, hydrolysis, and catalysis.[2,5,6,7] Heterogeneous catalysis is a promising method of lignin conversion due to its ability to separate products from the catalyst, and reducing the activation energy required for the reaction.

In trying to understand the reactivity of lignin, an approach has been taken to select small molecules as representatives of lignin fragments and progressively add complexity to these molecules approaching the complexity present in the lignin polymer. Previous studies of lignin valorization started with sample model molecules such as Phenol, Anisole, and 2-Phenoxyethanol.[8,9,10,11] These molecules are the simplest representation of the β-O-4 linkage present in large numbers in lignin. To increase the lignin model complexity, molecules bearing two methoxy functional groups on the 1,2, 1,3, and 1,4 positions, are used as models of the substituted adjacent β-O-4 linkage. These molecules are veratrol, 1,3-dimethoxybenzene, and 1,4-dimethoxybenzene (Figure 4.1).

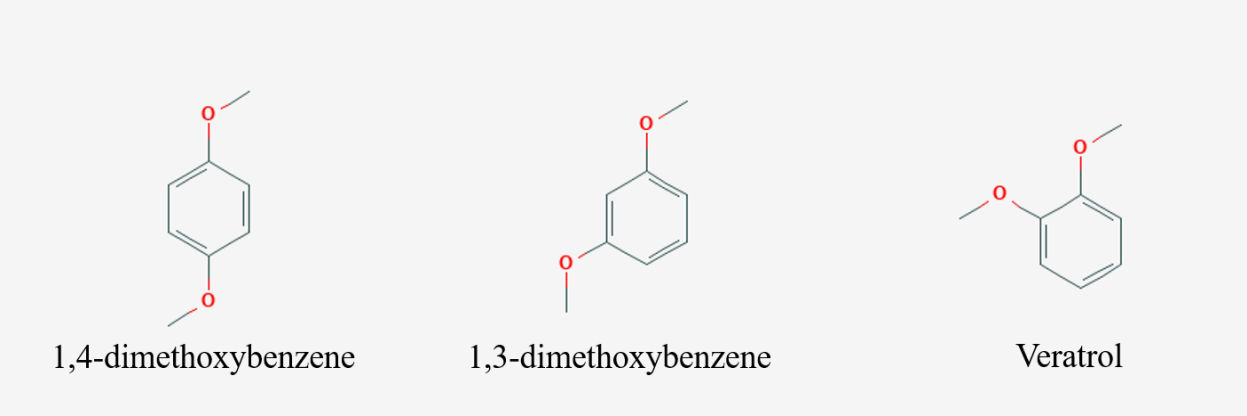

Figure 4.1: *The three molecules of Veratrol family.*

Giorgi and Co-workers studied veratrol on Pt(111) by a combination of three surface science techniques, X-ray Photoelectron spectroscopy, infrared reflection absorption spectroscopy, and temperature programmed desorption.[12] Veratrol was adsorbed on the surface at 130 K with two major signals in the C1s region at 285.2 eV and 283.5 eV corresponding to carbon atoms bound to an oxygen atom and carbon atoms bound to carbon atom, respectively. Desorption of physisorbed layer was observed at 215 K. while the monolayer decomposed by dehydrogenation of the methyl group below 300 K. 1,2-benzoquinone seems to be the intermediate in the decomposition pathway of veratrol. The observed byproducts are H_2 and CO.[12]

Since no experimental or theoretical work has been done for 1,3-dimethoxybenzene and 1,4-dimethoxybenzene with regard to their reactivity on single crystal catalysts, we compare the reactivity and the decomposition pathway of 1,3-dimethoxybenzene and 1,4-dimethoxybenzene with 1,2-dimethoxybenzene (Veratrol) by building on previous studies of veratrol on Pt(111). This study is conducted using infrared reflection absorption spectroscopy (IRAS) on Pt(111) surface.

4.2. Experimental

Experiments were performed under UHV conditions (pressure ≈ $1x10^{-10}$ mbar). The UHV regime is achieved by a combination of a mechanical pump and a turbomolecular pump. The chamber is designed for the Infrared reflection adsorption spectroscopy based on FTIR (Bruker Equinox 55) coupled with UHV chamber with a grazing reflection angle on the sample (detailed on Chapter 2 Section 4). The chamber contains a sputtering gun to clean the surface and a quadrupole mass spectrometer for residual gas analysis.

The experiments started with cleaning the sample (Pt(111) single crystal) via three repetitive cycles of sputtering of argon ions for 30 minutes at 600 K (1.5 keV, 1 x 10-5 mbar Ar+), followed by annealing for two minutes at 1100 K after each cycle. After sample cleaning, the sample cooled down by liquid nitrogen to deposit the molecules at the lowest temperature (about 120-130 K).

Veratrol (99% purity, Sigma-Aldrich), 1,3-dimethoxybenzene (≥98% purity, Sigma-Aldrich), and 1,4-dimethoxybenzene (99% purity, Sigma-Aldrich) were dosed to the chamber through a leak valve, the leak valve is attached on the chamber for dosing molecules into the chamber. The lines heated up to 200^0 in order to increase the vapour pressure and to ensure a pure molecule introduced into the chamber.

The collection of spectra was done by the OPUS software at 4 cm^{-1} with 1000 scans. The first spectrum acquired at~130 K then heated up to desired temperatures and acquired spectra at different temperatures. Spectra were manipulated by OPUS software to correct the baseline and to remove the atmospheric distribution for CO_2 and H_2O.

The calculation modes in tables (4.1) and (4.2) are obtained from WebMO. The Gaussian program was used at the B3LYP/6-31G(d) level for isolated molecules in gas phase at the room temperature. The calculation involved a geometry optimization of the idealized molecule followed by a vibrational frequency calculation of the optimized geometry. The focus of these calculations is not absolute accuracy of vibrational frequencies, but rather to identify the main groups involved in the vibrational modes of the molecules.

4.3. Results

IRAS spectra were obtained for veratrol, 1,3-dimethoxybenzene and 1,4-dimethoxybenzene upon the adsorption of a multilayer on Pt(111). Data was then obtained as a function of temperature and the spectra were analysed using the OPUS software.

4.3.1. Veratrol

Veratrol has been discussed in detail in chapter 3. Here the IRAS analysis is presented briefly for comparison with its isomers. Veratrol shows seven major peaks on its vibrational spectra after deposition of 200 L at 130 K. The seven peaks appear in the spectra at 758, 1033, 1127, 1261, 1467, 1515 and 1595 cm^{-1}. The peaks at 1515 and 1595 cm^{-1} are assigned to C-C ring + CCO stretches and the peak at 758 cm^{-1} to C-H bending out of plane. The more relevant peak assigned to O-CH_3 stretching is observed at 1033 cm^{-1}. The Ph-O + C-C stretch is assigned at 1261 cm^{-1}. The peak at 1127 cm^{-1} corresponds to a CH bending mode. While the CH_3 scissoring is assigned at 1467 cm^{-1}. The strong observations of C-H bending peaks indicates that veratrol adsorbs initially on the surface via carbon atoms of the aromatic ring. With increasing temperature, the majority of peak intensities remain unchanged until at 240 K the peaks of the CH_3 fragment became stronger and sharper, which means the molecule starts to rearrange itself on the platinum

surface to a more thermodynamically stable geometry. At 300 K, the intensity of peaks goes down indicating that the multilayer of veratrol has been desorbed. The disappearance of CH_3 peaks and the constant presence of O-CH_3 and Ph-O+C-C stretching suggest that the molecule started decomposing by breaking C-H bonds on methyl group, as has been previously observed for anisole and 2-phenoxyethanol.[8-9-10] Upon heating to 330 K, desorption of the monolayer competes with decomposition and the disappearance of O-CH_3 stretching, CH_3 rocking, and CH_3 scissoring peaks indicate that veratrol decomposition leads to the formation of 1,2-benzoquinone species on the surface. Further heating to 400 K, the observed peaks at 758 cm^{-1}, assigned to C-H bending out of plane, gets stronger and a new peak emerges at 950 cm^{-1} which indicates the ring breaks down as veratrol completely decomposed. Above 400 K, the remaining peaks disappear emphasizing that the molecule has been decomposed.

The identification of surface species upon dosing multilayers of veratrol on Pt (111) was performed by monitoring vibrational modes of species on the surface as a function of temperature. Details of the band assignments and comparison to the vibrational frequencies of liquid anisole are presented in chapter 3.

The XPS data emphasized that the desorption of veratrol's physisorbed layer is around 260 K when the intensity of C-C and C-O peak areas decrease in the C 1s region. The spectra of TPD also shows at 215 K the multilayer desorbed. In the O 1s region of XPS, the peak area intensity decreased and shifted to a lower binding energy of 531.3 eV, leading to the desorption of monolayer at 360 K. Turning to TPD data, the byproducts observed in veratrol decomposition pathway are H2, CO, and catechol (formed by hydrogenation of 1,2-benzoquinone). While the 1,2-benzoquinone seems to be the key intermediate of the molecule decomposition pathway. Desorption of catechol and carbon monoxide correlates with the disappearance of the C-O peak in

C 1s and in the O 1s region at 360 K, and the appearance of a new peak at 950 cm^{-1} indicates further decomposition of the 1,2-benzoquinone.

4.3.2 1,3-dimethoxybenzene

Figure 4.2 shows the vibrational spectra of 1,3-dimethoxybenzene after dosing 200L at 130 K, with acquiring spectra at different temperatures. Upon deposition at 130 K, the 1,3-dimethoxybenzene shows eight major peaks in the spectra at 772, 1053, 1160, 1215, 1270, 1290, 1497, and 1608 cm^{-1}. The peaks at 1608 and 1497 cm^{-1} are assigned to C=C stretching, 772 cm^{-1} to C-H bending out of plane and 724 cm^{-1} to ring breathing. The peak at 1054 cm^{-1} is assigned to C-H bending. The peak at 1215 cm^{-1} is assigned Ph-O antisymmetric stretch. The peak at 1160 cm^{-1} is assigned to C-O-C antisymmetric stretch. While the peaks 1290 and 1270 cm^{-1} corresponded to C-C stretch and Ph-O antisymmetric stretch, respectively. Weak peaks at 3007 and 2983 cm^{-1} are assigned to CH_3 antisymmetric stretching. A relevant peak at 2836 cm^{-1} assigned also to CH_3 but stretching symmetrically. Two peaks at 690 and 840 cm^{-1} assigned to C-H bending out of plane.

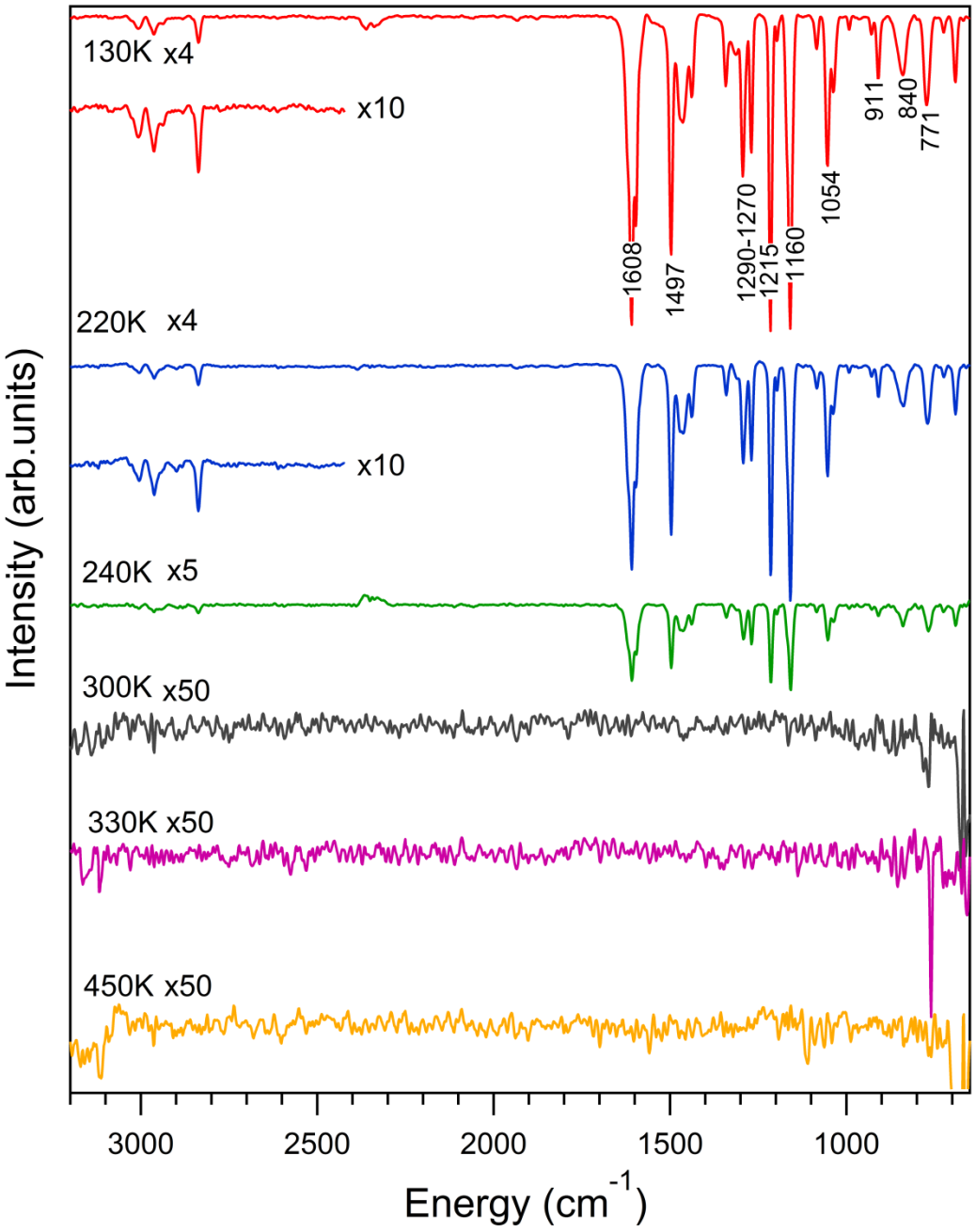

***Figure 4.2**: IRAS spectra acquired at different temperatures for 200L of 1,3-dimethoxybenzene.*

Details of the band assignments of the vibrational frequencies of liquid (experimental) and gas (calculated) phases of 1,3-dimethoxybenzene are presented in Table 4.1.

Table 4.1: *Vibrational modes and peak assignments of 1,3-dimethoxybenzene on Pt(111), on a Platinum electrode[14] and as calculated for gas phase molecules.*

Vibrational mode	Pt(111)	Liquid Phase (exp)[14]	Gas Phase (Cal)
(a) Arm vibrations			
CH_3 antisym. str.	**3007**	**3008**	**3160**
CH_3 antisym. str.	**2983**	**2969**	**3090**
CH_3 sym. str.	**2836**	**2840**	**3027**
CH_3 rock	**1197**	**------**	**1186**
C-O-C antisym. Str.	**1160**	**1190**	**1190**
C-O-C sym. Str.	**1037**	**1032**	**1078**
(b) Ring vibrations			
C=C stretch	**1608**	**1600**	**1668**
C=C stretch	**1596**	**1573**	**1548**
C=C stretch	**1497**	**1489**	**1517**
C=C stretch	**1463**	**1489**	**1485**
C=C Stretch	**1438**	**------**	**1389**
C-H sym. Def.	**1341**	**1379**	**1333**
C-C stretch	**1290**	**------**	**1318**
Ph-O antisym. Str.	**1270**	**------**	**1253**
Ph-O antisym. Str.	**1215**	**------**	**1205**
C-H bend	**1084**	**------**	**1080**
C-H bend	**1054**	**------**	**1092**
C-H rock	**992**	**------**	**1010**
C-H bend	**928**	**------**	**958**
C-C sym. Str	**910**	**918**	**936**
C-H bend (out of plane)	**840**	**------**	**847**
C-H bend (out of plane	**771**	**------**	**773**
Ring breathing	**724**	**------**	**738**
Ph-H bend (out of plane)	**690**	**------**	**695**

[a]Approximate mode description; str, stretching; sym/asym, symmetric/asymmetric; ip, in plane; op, out of phase.

There are some shifts between the vibrational modes of 1,3-dimethoxybenzene adsorbed on Pt(111) and those listed in the literature for the gas phase molecule and for the liquid molecule interacting with a platinum electrode. This is not surprising since the adsorbed species at 130K under UHV conditions is a condensed phase that has gas, liquid and solid qualities as well as a significant interaction with the metal surface. Nevertheless, the correlation of the observed peaks in the spectra can be used as a guide for peak assignment to the corresponding vibrational modes. Only the modes that have vibrational dipole moment perpendicular to the surface can be observed due to the surface metal selection rule, and this gives an insight about the geometry of the absorbent on the metal surface. The observation of the strong peaks at 690, 772, 840, and 1053 cm^{-1} that correspond to C-H bending mode indicates that the 1,3-dimethoxybenzene adsorbs on the surface primarily by the carbon atoms of the aromatic ring. Besides that, the observation of C-O-C stretch, Ph-O antisymmetric stretch means the methoxy group of the molecule is tilted from the surface. These observations are in agreement with the previous studies of similar molecules; anisole and veratrol on Pt(111).

Upon reaching 240 K, the IR peaks decrease in intensity significantly which indicates the multilayer of the 1,3-dimethoxybenzene has been desorbed. Now at 300 K, most IR peaks are disappearing that indicating largely monolayer desorption from the surface. The peak at 771 cm^{-1} that corresponds to C-H bending split into two peaks 781 and 767 cm^{-1}. The molecule most likely forms benzene on the surface rather than resorcinol (what I expected) because of the observations of C-H bonds in the aromatic ring.

Upon heating to 330 K, the only observed peak in the spectrum is 759 cm^{-1} that corresponds to C-H bending out of plane shifts from 771 and gets stronger. Up to 450 K, the remaining peak vanishes to conclude to the fully decomposition of 1,3-dimethoxybenzene on the surface. The

molecule behaves similarly like anisole. Plus, no molecular CO peaks in stretching mode have been observed at the region of 1800-2100 cm^{-1}, which suggests the desorption of CO from 1,3-dimethoxybenzene is reaction limited.

4.3.3 1,4-dimethoxybenzene

Figure 4.3. shows the vibrational spectra of 1,4-dimethoxybenzene after dosing 2000 L at 130 K, with acquiring spectra at different temperatures. Upon deposition at 130 K, the 1,4-dimethoxybenzene shows five major peaks in spectra at 723, 831, 1047, 1241, and 1513 cm^{-1} in the spectra. The peak at 1513 cm^{-1} corresponds to C=C stretching, and the peak at 723 cm^{-1} to Ph-O antisymmetric stretch. Two peaks at 1047 and 1241 cm^{-1} are assigned to C-O-C antisymmetric stretch. The peak at 831 cm^{-1} is assigned to C-H bending out of plane. Weak peaks are assigned CH_3 symmetric stretch at 2955 and 2835 cm^{-1}, and CH_3 antisymmetric stretch is assigned at 3004 cm^{-1}. Two peaks at 760 and 669 cm^{-1} correspond to C-H bending out of plane. A peak corresponds to C-C stretching at 1298 cm^{-1}. However, no conclusive O-H stretch peak can be attributed in the acquired spectrum.

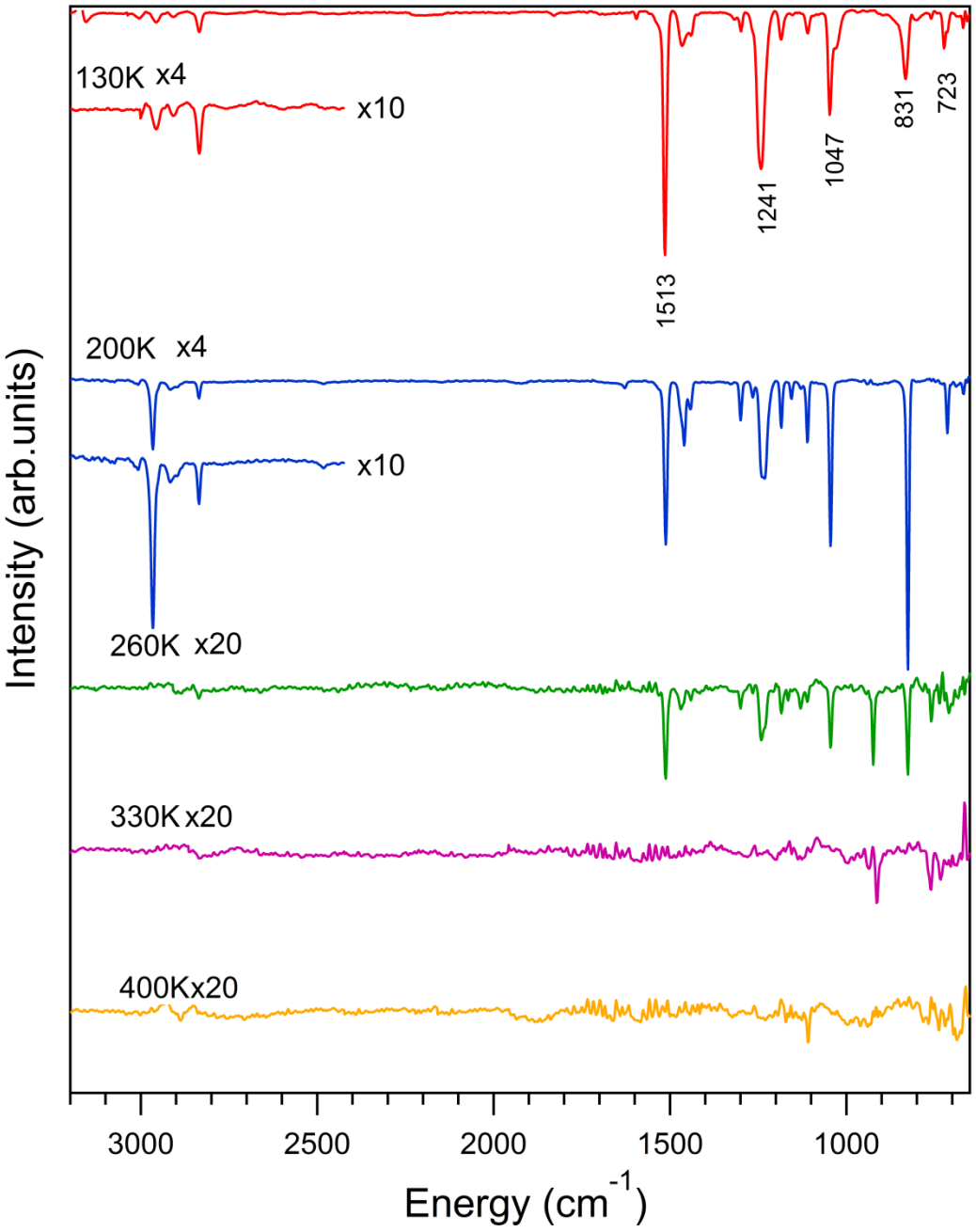

Figure 4.3: *IRAS spectra acquired at different temperatures for 2000L of 1,4-dimethoxybenzene.*

Details of the band assignments of the vibrational frequencies of liquid (experimental) and gas (calculated) phases of 1,4-dimethoxybenzene are presented in Table 4.2.

Table 4.2: *Vibrational modes and peak assignments of 1,4-dimethoxybenzene on Pt(111), on a Platinum electrode*[15] *and as calculated for gas phase molecules.*

Vibrational mode	Pt(111)	Liquid Phase (exp)[15]	Gas Phase (Cal)
(a) Arm vibrations			
CH_3 antisym. str.	**3004**	**3014**	**3152**
CH_3 sym. str.	**2955**	**2953**	**3018**
CH_3 sym. str.	**2835**	**2838**	**3017**
CH3 sym. Def.	**1465**	**1496**	**1538**
CH3 antisym. Def.	**1439**	**1440**	**1520**
C-O-C antisym. Str.	**1241**	**1250**	**1281**
CH_3 rock	**1184**	**------**	**1220**
C-O-C antisym. Str.	**1047**	**1040**	**1091**
(b) Ring vibrations			
C=C stretch	**1513**	**1520**	**1567**
C-C stretch	**1298**	**------**	**1375**
C-H bend	**1110**	**------**	**1139**
C-H bend (out of plane)	**831**	**------**	**843**
C-H bend (out of plane	**760**	**------**	**805**
Ph-O antisym. Str.	**723**	**------**	**731**
C-H bend (out of plane)	**669**	**------**	**533**
Ring breathing	**657**	**------**	**529**

[a]Approximate mode description; str, stretching; sym/asym, symmetric/asymmetric; ip, in plane; op, out of phase.

As for the other molecules, there are some shifts between the vibrational modes of gas, liquid and adsorbed 1,4-dimethoxybenzene. In addition pronounced shifts may be observed due to

the adsorbed/metal interaction, especially for the C-O−C peak that is shifted from 1250 to 1241 cm^{-1} which indicates that the surface influences the adsorption geometry of the molecule. There are also small shifts between the two liquids of 1,4-dimethoxybenzene because of two different catalysts Pt(111) and Platinum electrode. Only the modes that have vibrational dipole moment perpendicular to the surface can be observed due to the surface metal selection rule, and this gives an insight about the geometry of the absorbent on the metal surface. The observation of the strong peak 1513 cm^{-1} of carbon double bonds and the peak at 831 cm^{-1} that corresponded to C-H bending mode indicates that the 1,4-dimethoxybenzene adsorbs on the surface primarily via its carbon atoms of the aromatic ring. Furthermore, the observation of Ph-O and C-O-C antisymmetric stretch means the methoxy group of the molecule is tilted from the surface. This means all molecules of the Veratrol family have a similar adsorption behavior on Pt(111).[12]

Heating up to 200 K, the peaks in the C-H stretch regions get stronger and sharper due to the molecule rearranging itself in the adsorbed layer to a more thermodynamically stable geometry. Some peaks get stronger like the one at 831 and 1047 cm^{-1} with increasing temperature up to 200 K which means the desorption of multilayer does not occur yet. After increasing the temperature to 260 K, the intensity of IR peaks decreased, attributed to multilayer desorption. The peaks corresponding to CH_3 modes in C-H stretch region vanish and the constant presence of the 1047 and 1241 cm^{-1} assigned to O-CH_3 stretching and Ph-O + C-O-C antisymmetric stretching suggests that the 1,4-dimethoxybenzene started decomposing by C-H bond cleavage on the methyl group.

Further heating to 330 K, the IR peaks intensity further decreases leading to the desorption of monolayer of 1,4-dimethoxybenzene. Just a peak observed at 760 cm^{-1} corresponded to C-H bending out of plane which suggests the ring breaks down as the molecule decomposes. At 400 K,

the remaining peak at 760 cm-1 disappears, indicating the eventual full decomposition of the molecule on the surface.

Finally, no molecular CO stretching peak has been observed in the 1800-2100 cm^{-1} region, which suggests that the reported desorption of CO from 1,4-dimethoxybenzene decomposition is reaction-limited.

4.4 Discussion

Veratrol, 1,3-dimethoxybenzene and 1,4-dimethoxybenzne adsorb on the surface at 130 K. Upon heating, the decomposition pathways of these molecules undergo several bond cleavages. A summary of the decomposition pathways as determined by combining IRAS results with previous chapters is shown in Figure 4.4.

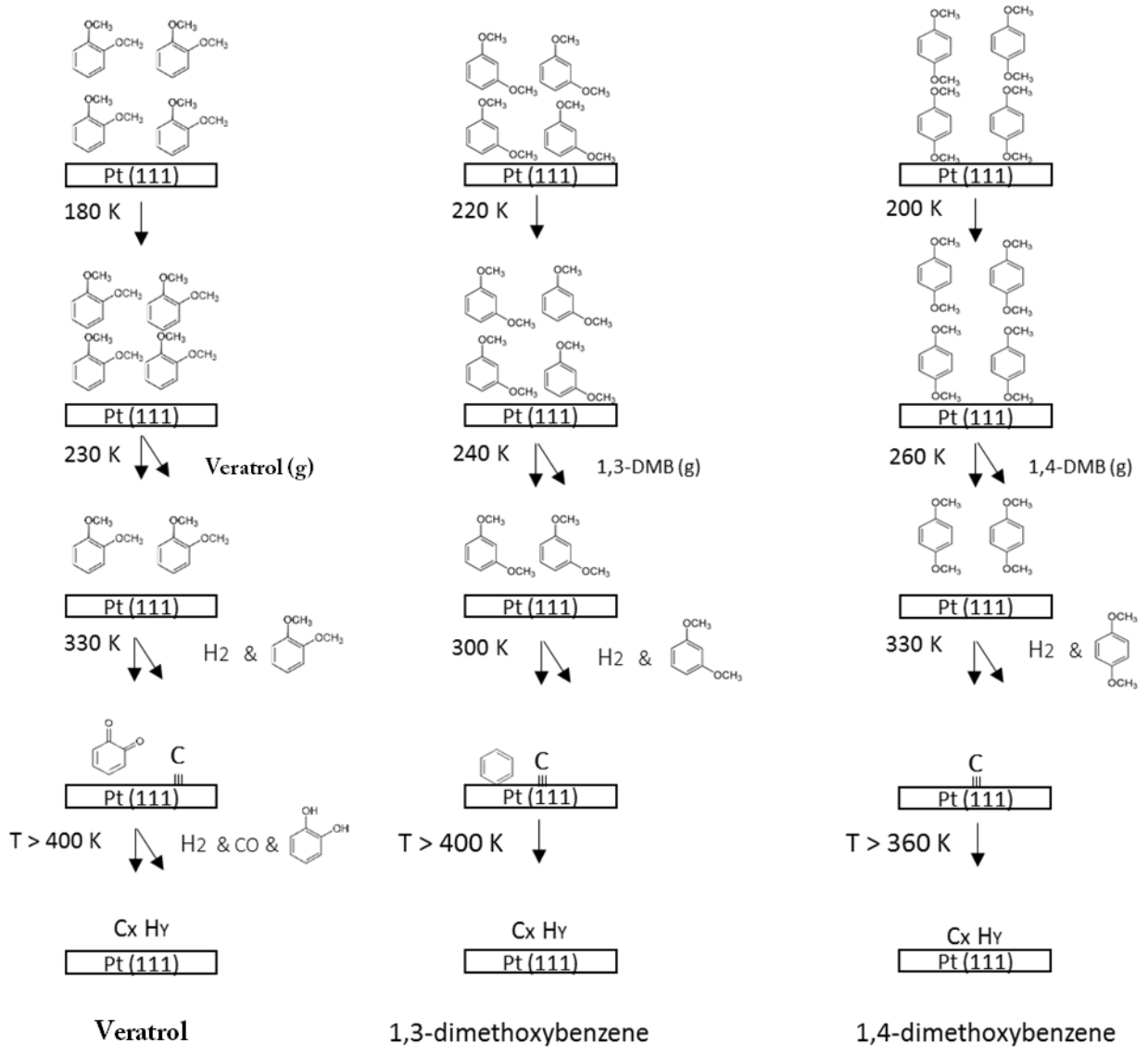

Figure 4.4: *The decomposition pathways of Veratrol and associated temperatures for, 1,3-dimethoxybenzene, and 1,4- dimethoxybenzene on Pt(111) under UHV conditions.*

Desorption

Veratrol desorbs form the surface in two steps: the multilayer desorbs at 230 K, while the monolayer desorption occur upon reaching 330 K. The reported TPD results showed the desorption energy of veratrol's physisorbed layer is 64.8 kJ/mol.[12] For guaiacol which is expected to behave

similarly, Vohs and coworkers showed, the multilayer of guaiacol desorbs from Pt(111) surface at 225 K. The reported XPS data confirmed at 360 K the monolayer of veratrol desorbed.[16]

1,3-dimethoxybenzene desorbs from the surface in two steps. The multilayer and the monolayer layer desorb from the surface upon reaching 240 K and 300 K respectively. These observations are similar to the reported IRAS results for anisole (240 K and 300 K for the multilayer and monolayer, respectively).[8] Also for anisole, the TPD results reported that the multilayer and part of the monolayer desorb at 260 K and 360 K respectively.[9]

The adsorption geometry of 1,4- dimethoxybenzene is different from the monolayer. The stronger observation of methyl group at 200 K, suggests the molecule has enough energy to reorient itself on the platinum surface upon heating to 200 K. The multilayer starts desorbing at 260 K, whereas the desorption of monolayer occurs upon heating to 330 K.

Decomposition

Veratrol decomposes its monolayer by the cleavage of methyl group above 330 K. This remark indicates the formation of 1,2-benzoquinone on the surface. A related study by McEwan and coworkers showed, guaiacol on Pt(111) at 375 K starts decomposing by either the dehydrogenation of the hydroxyl group or the methyl group to form 1,2-benzoquinone as key intermediate.[17] The observed byproducts of veratrol are catechol, H_2, CO.

1,3-dimethoxybennzene adsorbs to Pt(111) surface via carbon atoms of the aromatic ring. In the decomposition route of 1,3-dimethoxybenzene, the molecules decomposes by a C-H cleavage on the methyl group at 330 K as reported for similar molecules, anisole and veratrol.[9,8,12] 1,3-dimethoxybenzene most likely forms benzene on the surface as methoxy species are not

observed below 330 K, and the observation of C-H bending mode at 771cm-1. The only byproducts expected to be observed are H_2 and CO.

For 1,4-dimethoxybenzene, determination of intermediates was not forthcoming, and the expected observed byproducts were H_2 and CO. No alcohol or quinone species was observed in the IRAS spectra.

4.5 Conclusion

Under ultra-high vacuum conditions, the complex lignin model molecules, veratrol, 1,3-dimethoxybenzene and 1,4- dimethoxybenzene adsorbed on the Pt(111) surface at 130 K. The three molecules desorb their physisorbed layer between 230-260 K. The monolayer for the veratrol family gets desorption at 330 K. The para and ortho isomers showed some similarity in their reactivity. The adsorption geometries of the whole family are similar, namely via the interactions of carbons in the benzene ring with the Pt(111) surface. The common byproducts of the whole family are H_2 and CO. No alcohol was observed from 1,3-dimethoxybenzene and 1,4-dimethoxybenzene, while veratrol produced catechol after forming 1,2- benzoquinone as key intermediate of its decomposition. Current work involves additional surface science experiments on Pt(111) to be able to distinguish the intermediate species of the whole family and observe the byproducts of each molecule.

References:

(1) Pettersen, R. C. The Chemical Composition of Carbohydrates of Wood Cells. *J. Polym. Sci.* **2003**, *207*, 57–126.

(2) Kang, S.; Li, X.; Fan, J.; Chang, J. Hydrothermal Conversion of Lignin: A Review. *Renew. Sustain. Energy Rev.* **2013**, *27*, 546–558.

(3) Demirbas, A. Biomass Resource Facilities and Biomass Conversion Processing for Fuels and Chemicals. *Energy Conv*. Mgmt. **2001**, *42*, 1357−1378.

(4) Zakzeski, J.; Bruijnincx, P. C. A.; Jongerius, A. L.; Weckhuysen, B. M. The Catalytic Valorization of Lignin for the Production of Renewable Chemicals. *Am. Chem. Soc.* **2010**, *110*, 3552–3599.

(5) Jahirul, M. I.; Rasul, M. G.; Chowdhury, A. A.; Ashwath, N. Biofuels Production through Biomass Pyrolysis- A Technological Review. *Energies* **2012**, *5*, 4952 – 5001.

(6) Mohan, D.; Pittman, C. U.; Steele, P. H. Pyrolysis of Wood/Biomass for Bio-Oil: A Critical Review. *Energy and Fuels* **2006**, *20*, 848 – 889.

(7) Yan, N.; Zhao, C.; Dyson, P. J.; Wang, C.; Liu, L.-T.; Kou, Y. Selective Degradation of Wood Lignin Over Noble Metal Catalysts in a Two-Step Process. *ChemSusChem* **2008**, *1*, 626 – 629.

(8) Ould Hamou, C. A.; Giorgi, J. B. Direct Observation of Phenoxy as the Key and Common Intermediate for the Decomposition of Lignin Fragments Containing the β-O-4 Linkage. *J. Phys. Chem. C* **2018**. *123 (13)*, 8122-8132.

(9) Reócreux, R.; Ould Hamou, C. A.; Michel, C.; Giorgi, J. B.; Sautet, P. Decomposition Mechanism of Anisole on Pt(111): Combining Single-Crystal Experiments and First-Principles Calculations. *ACS Catal.* **2016**, *6*, 8166−8178.

(10) Ould Hamou, C. A.; Réocreux, R.; Sautet, P.; Michel, C.; Giorgi, J. B. Adsorption and Decomposition of a Lignin β-O-4 Linkage Model, 2-Phenoxyethanol, on Pt(111): Combination of Experiments and First-Principles Calculations. *J. Phys. Chem. C* **2017**, *121*, 9889−9900.

(11) Ihm, H.; White, J. M. Stepwise Dissociation of Thermally Activated Phenol on Pt(111). *J. Phys. Chem. B* **2002**, *104*, 6202–6211.

(12) Ould Hamou, C. A.; Asiri, M.; Kusuma, V.; Giorgi, J. B. Adsorption and Decomposition of a Lignin β-O-4 Linkage Model: Reactivity of Veratrol on Pt(111) by Combination of XPS, TPD and IRAS Experiments. **2019**, 1–20.

(13) Lucarelli, C.; Giugni, A.; Moroso, G.; Vaccari, A. FT-IR Investigation of Methoxy Substituted Benzenes Adsorbed on Solid Acid Catalysts. *J. Phys. Chem. C* **2012**, *116*, 21308–21317.

(14) Márquez, J.; Kalaji, M.; Hernández, R.; Márquez, O. P.; Martínez, Y. Electrosynthesis and Characterization of Poly(1,3-Dimethoxybenzene). *Synth. Met.* **2002**, *93*, 9–15.

(15) Choy De Martinez, M.; Márquez, O. P.; Márquez, J.; Hahn, F.; Beden, B.; Crouigneau, P.; Rakotondrainibe, A.; Lamy, C. In Situ Spectroscopic Investigation of the Anodic Oxidation of 1,4-Dimethoxybenzene at Platinum Electrodes. *Synth. Met.* **1997**, *88*, 187–196.

(16) Shi, D.; Vohs, J. M. TPD and HREELS Study of the Reaction of Guaiacol on Zn-Decorated Pt(111). *Catal. Today* **2018**, *302*, 272–276.

(17) Hensley, A. J. R.; Wöckel, C.; Gleichweit, C.; Gotterbarm, K.; Papp, C.; Steinrück, H. P.; Wang, Y.; Denecke, R.; McEwen, J. S. Identifying the Thermal Decomposition Mechanism of Guaiacol on Pt(111): An Integrated X-Ray Photoelectron Spectroscopy and Density Functional Theory Study. *J. Phys. Chem. C* **2018**, *122*, 4261-4273.

Chapter 5: Conclusion

5.1. Summary and Future Work

This study was a continuation of the previous studies of lignin valorization starting with three simple β-O-4 linkage models phenol, anisole and 2-phenoxyethanol. In my thesis, we increased the complexity of models by including two methoxy groups in the three positions 1,2, 1,3 , and 1,4. The target was to gain better understanding of the reactivity of lignin itself in order to exploit it eventually.

The methodology involved Infrared Reflection Absorption Spectroscopy for adsorbed molecules on a Pt(111) surface as a catalyst. For the simplest molecule, veratrol, we also used X-ray Photoelectron Spectroscopy and Temperature programmed Desorption on the same surface to provide additional insight. All experiments of this work were under ultra-high vacuum conditions.

In case of veratrol as an example, the multilayer of molecules desorbed at 215 K. veratrol kept decomposing by dehydrogenation of the methyl group until 300 K where the monolayer desorbed. Main products of the decomposition were Hydrogen, Carbon monoxide, and Catechol. We discovered the key intermediate of veratrol decomposition pathway was 1,2- benzoquinone.

Furthermore, comparing acquired data of 1,3-dimethoxybenzene and 1,4-dimethoxybenzene with veratrol leads to an insight of their reactivity. For the 1,3-dimethoxybenzene, the multilayer desorbs from the platinum surface at 240 K, and the monolayer at 300 K. The molecule most likely forms benzene species in its decomposition pathway. For the 1,4-dimethoxybenzene, the desorption of the molecule occurs in two steps; the multilayer and the monolayer desorb from the surface upon reaching 260 K and 330 K respectively. Carbon monoxide and hydrogen are currently the observed byproducts of these two isomers of veratrol family.

Adsorption geometries for the veratrol family have been studied trough this research. Indications are that the three isomers adsorbed initially via carbon atoms of the aromatic ring on Pt(111) surface. IRAS data gave enough results regarding to the geometrical adsorption of studied molecules.

The increase in molecular complexity from methoxybenzene to dimethoxybenzene leads to new reactivity. For example the additional substitution leads to the observation of alcohol (catechol from veratrol), which was not observed before in previous studies of the mono-substituted molecules. This discovery emphasizes the significant of increasing the complexity of model molecules.

In this thesis, we studied the adsorption and decomposition of the veratrol family of molecules (dimethoxybenzene isomers) as models for lignin fragments containing β-O-4 linkage. Furthermore, it would be interesting to see the decomposition pathway of more complex family of molecules such as 2-hydroxyethyl-phenol and 2-methoxyphenyl-ethanol families.

Since lignin is a complex polymer, its route of investigation requires always increasing the level of complexity of models. This would be the remaining work in future to understand the different reaction pathways of lignin decomposition. Currently, 1,3-dimethoxybenzene and 1,4-dimethoxybenzene require additional experiments to obtain better understand in regards to their reactivity. They may produce alcohol as well as veratrol or they may not. TPD and XPS would be more than enough to distinguish the products and the full decomposition of these molecules.